AD610179

AIR FORCE INSTITUTE OF TECHNOLOGY

AIR UNIVERSITY
UNITED STATES AIR FORCE

EFFECT OF CHAMBER PRESSURE ON THE
PERFORMANCE OF A SMALL
REVERSE-FLOW ROCKET ENGINE

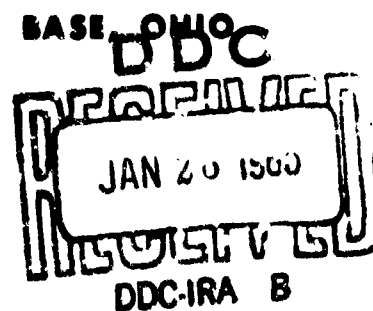THESIS

GA/ME/64-8   John C. Vaughan III
                     Capt   USAF

SCHOOL OF ENGINEERING

WRIGHT-PATTERSON AIR FORCE BASE, OHIO

EFFECT OF CHAMBER PRESSURE ON THE
PERFORMANCE OF A SMALL
REVERSE-FLOW ROCKET ENGINE

THESIS

GA/ME/64-8   John C. Vaughan III
                    Capt   USAF

EFFECT OF CHAMBER PRESSURE ON THE PERFORMANCE

OF A SMALL REVERSE-FLOW ROCKET ENGINE

THESIS

Presented to the Faculty of the School of Engineering of

the Air Force Institute of Technology

Air University

in Partial Fulfillment of the

Requirements for the Degree of

Master of Science

By

John Clark Vaughan III, B.S.

Capt   USAF

Graduate Astronautical Engineering

Summary

Experimental tests were made on a small reverse-flow rocket engine utilizing gaseous hydrogen and oxygen as propellants. The engine was operated at chamber pressures from 50 to 150 psia and developed thrusts from 40 to 150 pounds. The majority of tests were conducted at chamber pressures of 60 and 100 psia. Results indicated that the same maximum value of C* (7960 fps) and combustion efficiency (97%) were obtained for both these chamber pressures. However, with increasing chamber pressure the optimum mixture ratio increased. In addition, it was found that the best combustion chamber shape was spherical.

Preface

This report is one of a series of experimental studies by AFIT students on a reverse-flow rocket engine. The majority of my tests were made at chamber pressures of 60 and 100 psia where the effects of mixture ratio and engine size upon the characteristic exhaust velocity were investigated. The engine operated successfully during all tests and gave combustion efficiencies up to 97%. I hope that the results of this study will be of assistance to future investigators. I feel that many aspects of this type of engine are left to be examined.

I wish to acknowledge my indebtedness to Mr. John Parks for the many hours he willingly spent to assist me in the experimental work; to Lt. Tsongas, my advisor, for his support and guidance throughout this study; to Mr. Anderson, for his assistance in the digital computer work; and finally, a special thanks to my wife Patt for her help in editing and for her understanding and encouragement during the past eight months.

<div align="right">John C. Vaughan III</div>

Contents

I. List of Symbols

A   Area, in^2

B   Venturi diameter ratio (Throat diameter/Inlet diameter)

C*   Characteristic exhaust velocity, ft/sec

C_d Discharge coefficient

C_F Nozzle thrust coefficient

D   Diameter, in

E   Modulus of elasticity, psi

F   Thrust, lb

g   Gravitational conversion factor, 32.2 lbm ft/lbf sec^2

I_s Specific impulse, lbf sec/lbm

K   Thermal conductivity, BTU in/hr ft^2 F

k   Specific heat ratio (C_p/C_v)

L*   Characteristic length (V_c/A_t), in

L   Wall thickness, in

$\dot{m}$ Mass flow rate, lbm/sec

P   Static pressure, psia

q   Specific rate of heat flow, BTU/sec in^2

r   Mixture ratio, $\dot{m}_0/\dot{m}_H$

R   Specific gas constant (Universal gas constant/Molecular weight), ft lbf/lbm R

S   Tensile strength, psi

T   Temperature, F or R

V   Volume, in^3

Y_a Compressibility correction factor

α Coefficient of thermal expansion, in/in F

Δ Differential

ϵ	Nozzle expansion area ratio, A_e/A_t
η	Characteristic velocity quality factor, C^*_x/C^*_T, (Combustion efficiency/100)
λ	Thrust coefficient quality factor, C_{Fx}/C_{FT}
μ	Gas law deviation factor
γ	Poisson's ratio
ξ	Specific impulse quality factor, I_{Sx}/I_{ST}
ρ	Density, lbm/in^3
σ	Thermal stress, psi

Subscripts:

c	Combustion chamber
e	Nozzle exit
H	Hydrogen
O	Oxygen
p	Total propellants
s	Stagnation
T	Theoretical
t	Throat
x	Experimental

II. Introduction

Reverse-Flow Film Cooling

This study will consider the effect of chamber pressure on the performance of a small gaseous propellant rocket engine using reverse-flow film cooling. In this unique cooling system, a gaseous film of propellant travels at a relatively high speed along the combustion chamber inner wall toward the front of the chamber. It could be considered similar to re-generative cooling except that the propellant is in gaseous form and travels on the inside of the combustion chamber as it picks up heat.

The only known experimental work done with this type of cooling has been at the Air Force Institute of Technology. In the usual configuration, hydrogen gas is injected toward the front of the chamber from just upstream of the converging nozzle section. The coolant gas picks up heat from the combustion process as it proceeds to the front of the chamber. The relatively cool hydrogen gas film reduces the boundary-layer temperature, the heat transfer to the walls, and thus decreases the wall temperatures. At the chamber front the hydrogen converges on the gaseous oxygen injector where it mixes with the oxygen, and the combustion process begins. A cross section of the assembled engine is shown in Figure 1.

Applications

Probably the main disadvantage of such a cooling system is that one of the propellants must be injected in a gaseous

1

state and, therefore, requires large and heavy tankage for its storage (Ref 1:181). If the propellant were not stored in the gaseous state, but had to be vaporized just prior to injection, control problems would arise. Nonetheless, combustion of the propellant combination of gaseous oxygen/gaseous hydrogen can result in slightly higher specific impulse than the same liquid combination; thus, its high performance might offset the dis-advantages associated with its use. Of course, only the pro-pellant used for the reverse-flow film need be injected in a gaseous state; and, in fact, performance approaching that of theoretical has been achieved in a small uncooled engine using gaseous hydrogen and liquid oxygen (Ref 2).

Even though it is not the purpose of this study to pro-pose applications for a small thrust engine utilizing reverse-flow film cooling, it is useful to briefly consider one such example. A report titled "Closed Ecology" (Ref 3:4) shows that a completely closed respiratory system as might be used in extended, manned, space flights develops an excess of 0.2 lb/day of oxygen and 0.1 lb/day of hydrogen per man. These excesses could be used as the propellants for occasional veloc-ity corrections. It is possible that the duration of firing might be long enough to make an uncooled engine inapplicable. In addition, the required propellant flow might be too low for application of liquid regenerative cooling. Further, trans-piration and normal film cooling usually result in a loss of specific impulse--the amount of loss depending on the cooling requirements. Therefore, in such a situation, reverse-flow film cooling could have application.

2

Background Information

A complete survey was made of all work previously done with reverse-flow film cooled engines. The conclusions drawn from this survey, and presented below, were used in determining what ranges of chamber pressure, mixture ratio, characteristic length, and run time should be used in this study. Further, an attempt was made to take advantage of these previous results when considering what engine modifications would be necessary to prevent engine damage or would be helpful in increasing engine performance.

The original idea of utilizing a reverse-flow film to cool a small rocket engine was conceived by the personnel of the Fluid Dynamics Branch, Aeronautical Research Laboratory, Wright-Patterson A.F.B. A preliminary investigation as to the feasability of this idea was conducted by Guarino in 1958 (Ref 4). This was the first of twelve theses on topics dealing with reverse-flow film cooled engines. Guarino made test runs on a two dimensional, nine inch diameter circular chamber. Air was injected along the inside of the walls toward the front of the chamber at velocities up to 480 fps and at a flow rate of 0.5 lb/sec. A flow deflector was placed at the front of the chamber to turn the two air streams together and towards the exit. Results showed that the flow remained strongly attached to the wall until meeting the flow deflector. In addition, some of the flow appeared to recirculate in two vortices before leaving the chamber.

The following year, Morton (Ref 5) designed and operated

the initial reverse-flow engine. His basic design of a four inch diameter spherical combustion chamber of $\frac{1}{4}$ inch stainless steel walls has not been changed in subsequent studies. Gaseous hydrogen fuel was used for the film cooling and oxygen gas was the oxidizer. Both propellants were injected at sonic velocity to prevent possible chugging. The hydrogen was injected in a reverse-flow continuous annular stream and the oxygen injected in impinging streams that flowed directly rearward from a front injector. Six test runs were made at a chamber pressure of approximately 30 psia; the results showed that a reverse-flow film cooled small rocket engine could be successfully operated.

In 1960, Noland (Ref 6) verified Guarino's two-dimensional cold air flow results with the use of an interferometer. Injection velocities up to sonic were used. Chamber length was varied, and results showed that a circular configuration produced the strongest vortices, while a longer configuration produced the most stable flow pattern.

Additionally in 1960, a duplicate of Morton's engine was made so that experimental study could progress more rapidly. As of 1963, four studies were completed with the original engine and three with the other. All of these studies used hydrogen gas for the reverse-flow film (fuel) and oxygen gas for the oxidizer. Although the studies completed on the two engines were not independent of one another, they can be summarized as such.

With one of the engines, James (Ref 7) conducted a comprehensive performance study including many temperature

4

measurements. Sixty-nine test runs were made at chamber

pressures from 40 to 70 psia and mixture ratios from one to

eight. Temperature results indicated the reverse-flow film

to be an effective cooling scheme for runs of 35 seconds in

which both inside and outside wall temperatures reached

stable values. It was also shown that C* varied slightly

with chamber pressure for the one engine configuration tested.

In 1961 the construction and instrumentation of the AFIT

Rocket Engine Test Facility was completed by Macko, Keller,

and Pickitt. The facility was used for all subsequent rocket

engine tests. A complete description of the facility and its

instrumentation is given in an operation manual (Ref 8).

Macko (Ref 9) then continued the work of James in the

newly completed test facility. Engine sealing methods were

improved, several components were redesigned, and water cool-

ing was added to the nozzle divergent section. Two chamber

extensions were made to give four different L* configurations.

However, only ten test runs were made by Macko due to time

limitations.

In 1963 Johnston (Ref 10) extended the work of Macko and

James to investigate the effect of chamber length and oxygen

injector type on engine performance. One hundred and seventy-

five test runs were made at a nominal chamber pressure of 60

psia and mixture ratios of 1.3 to 4.4. Three different oxygen

injectors were tested, and L* was varied in configurations of

41.6, 56.7, 71.8, and 86.9 inches. Test results indicated

experimental values of C* well below theoretical C*. The engine

5

with an L* of 56.7 inches gave the best performance for all
injectors and was the only configuration in which maximum C*
did not occur at the lowest mixture ratio tested. The reason
postulated for the low values of C* was that the hydrogen was
incorrectly injected.

The series of studies using the duplicate engine was
started in 1960 by Krumpe (Ref 11). He used an impinging
stream oxygen injector and investigated the effect of inject-
ing the hydrogen with a component of swirl. The hydrogen in-
jectors used gave 0, 15, and 30 degrees of swirl. Fifty-one
test runs were made at a chamber pressure of 65 psia and
mixture ratios of one to three. The results showed that the
swirl injection gave higher C* but lower I_s values. For all
runs it was found that C* and I_s increased as the mixture
ratio decreased. It was believed that the exhaust gases still
had a component of swirl which decreased the axial component
of exhaust velocity, thus lowering the specific impulse.

The following year Keller (Ref 12) continued Krumpe's
work on swirl injection. Several important design changes
were incorporated; these included an improved hydrogen mani-
fold, a swirl oxygen injector, new swirl hydrogen injectors,
and a new exhaust nozzle. To aid in cooling the exhaust
nozzle, a hydrogen baffle was made to channel the incoming
hydrogen gas along the exterior of the nozzle. Keller only
made two test runs with the engine due to time limitations.

In 1962 Kineer (Ref 13) continued the study of swirl in-
jection; one hundred test runs were made at a chamber pressure

of 65 psia and mixture ratios ranging from 1.2 to 2.5. He used the swirl oxygen injector designed by Keller and a modification of Keller's hydrogen injectors with 0, 17, and 35 degrees of swirl. Characteristic lengths of 40 inches (spherical) and 55 inches (1 inch chamber extension) were used during his tests; run results for both engines showed that C^* increased slightly as the hydrogen swirl angle increased, but that I_s decreased with the increased swirl. Values of nozzle thrust coefficient unexplainably decreased for each injection angle when L* was increased from 40 to 55 inches. It was found that for mixture ratios less than 1.2 the oxygen injector face burned, and for mixture ratios higher than 2.5 the nozzle burned.

One year later Cunningham (Ref 14) extended the swirl injection studies to a comparison between swirl and shower-head oxygen injection. Characteristic length configurations of 44, 59, 74, and 90 inches were used. Sixty-six test runs were made at a chamber pressure of 60 psia and mixture ratios from one to three. The results showed that use of the shower-head injector gave higher values of C^* and I_s and lower wall temperatures than use of swirl injection. The best performance occurred with L* of 59 and 74 inches. For all L* configurations, C^* and I_s varied inversely with mixture ratio. The reverse-flow film cooled the chamber walls effectively, but the convergent portion of the nozzle was erosively burned at a mixture of 3.3.

In addition to the hydrogen-oxygen reverse-flow studies

7

just discussed, two reverse-flow studies were made using JP-4 and air as propellants. In 1960 Heye (Ref 15) conducted hot runs with a two-dimensional engine. Results showed that the reverse-flow film of air was effective in cooling the walls. In 1961 Agosta (Ref 16) tested a cylindrical engine. Chamber wall burning occurred, however, due to the fact that the injected fuel disrupted the reverse-flow air film and thus eliminated the local cooling effect.

One last group of studies by AFIT students is worth mentioning here. In 1960 Ow (Ref 17) designed and tested a gaseous oxygen-gaseous hydrogen, film cooled, rocket engine developing 100 pounds thrust at a nominal chamber pressure of 300 psia. The hydrogen was injected perpendicular to the chamber axis and hence reverse-flow film cooling was never utilized. This work was continued in 1961 by Pickitt (Ref 18) and in 1963 by Alser (Ref 19). The results of these studies showed that performance close to theorectical C* could be achieved in a small gaseous oxygen-hydrogen rocket engine and that the experimental C* varied with mixture ratio in a manner similar to the theoretical C* variation. Alser's study showed that adequate nozzle cooling could also be achieved by using normal film cooling, but with a resultant drop in C*.

In summary, it can be seen that a considerable amount of work has been done on a hydrogen-oxygen reverse-flow engine. The following results were compiled from these studies and were used in the planning and component design for this investigation:

1. Noticeably different flow patterns resulted when a spherical chamber was extended into a more cylindrical one.

2. The showerhead oxygen injector gave better performance and its use resulted in better chamber cooling than that obtained by swirl injection.

3. Except for James' study in which the effects of varying the chamber pressure between 40 and 70 psia were examined, all previous studies were conducted with a nominal chamber pressure of 60 psia.

4. With one exception, in all studies the mixture ratio was varied from one to three. At higher mixture ratios the convergent section of the nozzle suffered damage. James varied mixture ratio up to eight without burning, but at those mixture ratios above three his C* was less than 5000 fps. Previous studies had indicated that C* was approximately 6200 fps at mixture ratios of three, and therefore involved greater heat release.

5. All studies except Johnston's showed that C* decreased as mixture ratio increased. His study indicated that the configuration that gave the best performance had a C* versus mixture ratio curve which was similar in form to that found theoretically.

6. Although previous performance was low in comparison to theoretical C*, several studies showed that the performance was greatly affected by the type of oxygen injector. It was also shown that chamber length affected performance.

Problem Statement

The primary purpose of this thesis was to investigate the effect of chamber pressure on the performance of a small reverse-flow rocket engine. In order to limit the investigation, it was necessary to hold some factors constant. The first decision was to use the same hydrogen injector, oxygen injector, and exhaust nozzle throughout all performance tests. The second factor to consider was injection velocity of the propellants. Sonic injection was decided upon for two reasons. First, with one exception, all previous work had used this velocity and comparison could be made. Secondly, by using sonic injection, mass flow rates were independent of chamber pressure, thus allowing for easier control of mixture ratio and chamber pressure.

By fixing the injectors, nozzle, and injection velocities, the problem was reduced to three basic variables: chamber pressure, mixture ratio, and characteristic length. By holding any two of these constant, a relationship exists between the third variable and $C*$. Changing either of the first two variables would affect the relationship of the third to $C*$.

The variable of primary importance was P_c. It seemed that its range would be limited by the effectiveness of the cooling scheme. Although previously the engine had been tested at pressures up to 70 psia, for this study it was decided to investigate chamber pressure effects up to 300 psia.

The second variable was mixture ratio, which, it was felt, should be kept between one and three to prevent possible engine

damage. A possible exception would be to locate the peak of a C* versus r curve should it lie outside of this range.

The third variable to be considered was L*. Two chamber extensions were available. They, combined with the basic engine, allowed characteristic chamber lengths of 44, 60, 76, and 92 inches, providing the same A_t was used as in previous studies. Since Cunningham's results showed the optimum L* to be in the middle of this range, it was decided to use the same A_t and all the L* configurations available.

The final consideration in limiting the scope of investigation was the length of each run. It was found in previous studies that the chamber pressure, flow rates, and thrust would stabilize within two to three seconds. The only data which could not be determined with a run of three seconds duration were the steady state temperatures. Therefore, to conserve propellant, test runs would be limited to three or four seconds, except for a few long duration runs to determine heat flux and steady state wall temperatures.

III. Apparatus

Test Facility

The Rocket Engine Test Facility of the Mechanical Engineering Department was used for this study. Briefly, the main sections of the facility were the gas supply, the test cell, and the control room. The gas supply consisted of eight nitrogen, ten oxygen, and twenty hydrogen bottles. The test cell contained the engine and its test stand (Fig 8), propellant feedlines, flow control valves, and data pickups. The control room itself contained the data recorder and the control console (Fig 9). A complete description of the test facility is given in the Operations Manual (Ref 8).

Rocket Engine

Basic Engine Features. The basic combustion chamber consisted of two 4-inch diameter hemispheres with $\frac{1}{4}$ inch walls. The chamber shape and volume could be varied by inserting a one- and/or two-inch cylindrical extension between the hemispheres. A simplified stress analysis of this combustion chamber is given in Appendix A.

The other main engine parts were the nozzle, baffle, and injectors (Fig 1, 2). The exhaust nozzle had a throat diameter of 1.007 inches and an exit diameter of 1.179 inches. The resulting area ratio gave optimum expansion at a chamber pressure of approximately 60 psia. The brass baffle was the only main engine component which was not made of stainless steel. The baffle fit around the exhaust nozzle and allowed

a narrow channel between the baffle and nozzle for the in-
coming hydrogen flow; this provided regenerative cooling for
the nozzle. The engine was bolted together in such a way as
to allow removal of the injectors, nozzle, and baffle without
requiring disassembly of the combustion chamber. Modifica-
tions of the combustion chamber seals (Fig 3) and bolts are
discussed in Appendix B.

Exhaust Nozzle. Past studies showed that the nozzle was
the most critical component with regard to cooling. It be-
came obvious that measures had to be taken to prevent nozzle
damage during the proposed high pressure runs, as the heat
flux is almost proportional to the chamber pressure (Ref 20:
93).

A frequently successful method to protect parts in con-
tact with combustion gases is to coat the exposed areas with
a refractory liner (Ref 21:444). Such a coating was provided
and applied by the University of Dayton Research Institute
(Fig 4). The lining consisted of a flashing of nichrome and
then a 5 to 10 mil overcoat of Mullite. Mullite consists of
70% Al_2O- and 30% SiO_2 and has an orthorhombic crystal structure.
It has a density of 3.2 grams/cm^3 and a melting temperature of
3310 F. The thermal conductivity is very low--approximately
2 BTU/hr ft F. The coating was tested by subjecting it to a
2600 F plasma arc for five seconds; no cracks had occurred
after six such tests.

The thickest portion of the coating was applied to the
lip of the converging nozzle section where previous damage had

occurred and the thinest was applied at the throat section.
This was done for two reasons: first, the throat section is
cooled by the incoming hydrogen gas which is at its lowest
temperature; and second, as testing progressed, any flaking
of a thick coating at the throat would appreciably change the
throat area, which would complicate C* calculations.

Oxygen Injector. On the basis of Cunningham's compara-
tive study of swirl and showerhead injectors (Ref 14:50), it
was decided to use a modification of the latter. Previously
it had been found that C* increased as the mixture ratio was
reduced to one, whereas theoretical C* decreases. Such a
significant variation from theoretical C* was possibly due to
the center portion of the injected oxygen stream leaving the
combustion chamber without mixing and taking part in the com-
bustion. To correct this phenomenon, the center injection
holes were eliminated (the new injector is shown in Figures 5
and 6). The calculations used to determine the number and
size of injector holes which would keep the injection sonic
are contained in Appendix C.

Hydrogen Injector. Good results were achieved in the
past by injecting the hydrogen gas at Mach one and in a direc-
tion tangential to the chamber walls. Therefore, only two
modifications were made. First, it was decided to increase
the injection area because the previously used injector would
have required excessive line pressures to achieve higher flow
rates (Ref 14:31). It was found that the injection area
could be increased and still maintain sonic injection for all

14

the flow rates to be used. The calculations to determine the new injection hole size are included in Appendix C.

Secondly, it was decided to use a stainless steel injector so that it would have the same coefficient of thermal expansion as the nozzle. Having the same coefficient might eliminate the "necking down" of the exhaust nozzle (Ref 13:14), which was believed due to the expansion of the brass hydrogen injector. It should be noted that the final injector was a modification of that used by Krumpe in that the hydrogen flowed only through the new injector's outer ring of holes (Fig 7). The old inner ring of holes was purposely blocked by the baffle.

Engine Thermocouples. Each chamber extension and hemisphere had three iron-constantan thermocouples already installed. The thermocouples were circumferentially spaced at 120 degree intervals and measured the inside wall temperature. Additional iron-constantan thermocouples were installed to measure the corresponding outside wall temperature for use in temperature stabilization runs.

In addition, an unsuccessful attempt was made to measure the nozzle throat temperature with an alumel-chromel thermocouple. After a few test runs, the thermocouple was removed due to excessive hydrogen leakage from around it. No satisfactory sealing method could be achieved that would allow for the frequent removals necessary for engine inspection. Therefore, only chamber wall temperatures were recorded.

Propellant Feed System

Gaseous hydrogen and oxygen were used as propellants, while nitrogen gas was used for purge and for control pressure to the three flow regulating dome valves. These dome valves were designed to produce an engine feedline pressure equal to their respective control pressures. Loader valves on the control console regulated these control pressures and reduced the nitrogen supply pressure to the value desired at the respective dome valves. Thus, the hydrogen and oxygen propellant flows and the nitrogen purge flow could be regulated from the control console with only nitrogen lines being brought into the control room. The flow control system schematic is shown in Figure 10.

Instrumentation

All experimental run data was obtained from the output (Fig 11) of an eighteen channel Consolidated Electronics Corporation recorder. Thermocouples provided the electrical signal representing temperature changes, while bridge circuits were used to produce the thrust and pressure signals. Three types of galvonometers were used. Each type had a different sensitivity and required damping resistance. The sensitivities were high enough as not to require amplification of the input data signals.

The thrust signal input to the recorder came from a bridge of four active strain gauges mounted on a constant stress cantilever beam. Calibration was performed by hanging a known weight to the thrust beam and noting the trace

16

deflection at the recorder. Even though the calibration factor for any engine configuration was a constant for the ranges of thrust used, it was found that for any change of engine configuration the thrust beam had to be recalibrated. Further, for chamber pressures above 120 psia (high thrust), a less sensitive galvonometer had to be used to keep the deflection on the recorder paper. This method proved to consume less time than changing the fixed damping resistors.

The chamber pressure was measured with a transducer which was calibrated several times by applying a known pressure. The calibration factor was found to be a constant for the range of chamber pressures investigated and remained constant for the duration of the study.

Two Herschel tube venturi meters were used in obtaining the hydrogen and oxygen mass flows. The necessary pressures were obtained using static and differential pressure transducers. These transducers were calibrated in the same manner as the chamber pressure transducer.

The instrumentation system just described contained two improvements over the one used previously. First, in order to eliminate variation of supply voltage to the pressure transducer and thrust beam bridge circuits, a large aircraft battery was used for the power source. The battery voltage, 12 volts, was reduced to 10 volts with a variable resistor. This voltage was continually measured by a voltmeter located near the recorder. Second, the fixed damping resistors used in the thrust and pressure channels gave improved system reliability over the amplifiers used before.

17

All the engine wall temperatures and the two propellant venturi temperatures were measured with iron-constantan thermocouples. Each electrical circuit to the recorder consisted of a data junction, a cold junction ice water bath, and a series variable resistor. The variable resistor was used to adjust the calibration factor for the circuit while approximately giving the external damping resistance required by the galvonometer of that channel.

IV. Test Program

Test Schedule

Phase I. The first of two phases of testing, consisting of 43 runs, was mainly conducted to compare the new oxygen and hydrogen injectors to the ones used previously. All possible engine-injector combinations were tested. Mixture ratios were varied from one to two and chamber pressures from 54 to 132 psia. These first tests were also used to check the functioning of the instrumentation and the propellant feed system and the soundness of other engine modifications.

Phase II. The last phase of testing consisted of runs 44 to 119. The same oxygen injector, hydrogen injector, and exhaust nozzle were used for all of these tests (see Fig 5, 7, and 4 respectively). The four engine configurations were tested with mixture ratios from 0.94 to 3.5 and chamber pressures from 55 to 150 psia. However, the majority of tests were conducted at nominal chamber pressures of 60 and 100 psia. Due to insufficient supply pressure, stable hydrogen flows above 0.2 lbm/sec were hard to achieve; therefore, only a limited number of runs were made at chamber pressures above 120 psia.

Run Procedure

The same procedure was used in conducting all test runs. A small hydrogen flow was started and then electrically ignited outside the combustion chamber. Oxygen flow was then started and increased until the flame would progress into the

chamber and give a distinctive "pop". At this time the preset
run control pressures were applied to the hydrogen and oxygen
dome valves. The propellant flow would reach a steady value
in approximately two seconds. Unless a temperature stabiliza-
tion run were being made, engine purge and shut down would be
initiated after three seconds of run time. The run checklist
used for all runs is included in Appendix D.

V. Data Reduction

Engine Performance Parameters

The main parameter used to evaluate the performance of the rocket engine was the characteristic exhaust velocity, $C*$. The experimentally determined value, $C*_x$, was calculated for each run from the equation

$$C*_x = P_c A_t g / \dot{m}_p \tag{1}$$

In addition to $C*_x$, the other performance parameters were computed by use of the following equations:

$$C_{Fx} = F / P_c A_t \tag{2}$$

$$I_{sx} = C_{Fx} C*_x / g \tag{3}$$

$$\eta = C*_x / C*_T \tag{4}$$

$$\lambda = C_{Fx} / C_{FT} \tag{5}$$

$$\S = \eta \lambda = I_{sx} / I_{ST} \tag{6}$$

Computer Program

A digital computer was used to calculate the performance parameters for all test runs. The complete details of the computer program are given in Reference 22.

For each test run the computer used three sets of information. The first set consisted of eight calibration factors and the exhaust nozzle throat diameter. The calibration factors were given in lbf, psi, or F per inch of deflection. The second set of information consisted of the run number,

21

GA/ME/64-8

eight measured deflections, the mercury barometer reading, and the mercury temperature reading. The eight measured deflections were taken from the following recorder channels: thrust, chamber pressure, hydrogen feedline pressure, hydrogen venturi differential pressure, oxygen feedline pressure, oxygen venturi differential pressure, hydrogen feedline temperature, and oxygen feedline temperature.

The machine then computed and typed out the following data results: run number, F, P_c, r, C_X^*, C_{Fx}, I_{s-}, P_h, ΔP_H, P_0, ΔP_0, T_H, T_0, $\dot{m}_H$, and $\dot{m}_0$. At this time the computer was given the third set of information which consisted of C_T^* and C_{FT} values obtained from Figures 12 and 19. These curves of theoretical performance were plotted from the results of a digital computer program (Ref 22) using the following assumptions: frozen equilibrium, ambient pressure of 14.7 psia, expansion area ratio of 1.3707, and a conical nozzle with a 15 degree divergence half angle. The machine then calculated η, λ, and $\S$ and punched a summary card. The listings of all the Phase II test run performance summaries are given in Tables I to IV.

Mass Flows

The mass flow rates were computed by using the standard equation

$$\dot{m} = 0.525 Y_a C_d D_t^2 (P \Delta P)^{\frac{1}{2}}/(1-B^4)^{\frac{1}{2}} \tag{7}$$

22

where:

$B = 0.575$

$D_t = 0.376$

$C_d = 0.984$

$Y_a = (1-0.644 \, \Delta P/P)$

The discharge coefficient was obtained by calibrating the venturi meters against three standard square-edged orifices, using standard A.S.M.E. procedures (Ref 8:38). The accuracy of the calibration data is within $\frac{1}{2}\%$ for Reynolds numbers above 80,000. Since this Reynolds number corresponds to a $\dot{m}_H$ of 0.021 lbm/sec and a $\dot{m}_0$ of 0.046 lbm/sec, all test runs were above an 80,000 Reynolds number, and the constant C_d value was valid.

The curve of Y_a versus the throat to upstream static pressure ratio is almost a straight line for the meters used and can be approximated as shown above. This approximation introduces less than 0.2% error for throat to upstream static pressure ratios greater than 0.85. This pressure ratio was higher than 0.90 for all runs of this study.

By using a reference temperature of 100F, the flow equation can be reduced to the final form:

$$\dot{m}_H = 0.001419\left(1-0.644 \, \frac{\Delta P_H}{P_H}\right)\left(P_H \, \Delta P_H \, \frac{560}{T_H}\right)^{\frac{1}{2}} \tag{8}$$

$$\text{and } \dot{m} = 0.00565\left(1-0.644\frac{\Delta P_0}{P_0}\right)\left(P_0 \, \Delta P_0 \frac{560}{T_0}\right)^{\frac{1}{2}} \tag{9}$$

Temperatures

In order to achieve a fairly common basis for comparison, the temperatures for all short runs were measured after 3.0 seconds of run time. Since these temperatures were usually not steady state values, only very general conclusions could be drawn from them. Any possible trends were further disguised since the engine temperatures at run start varied from ambient temperature for the first run of the day to almost steady state temperature for a normal run immediately following an extremely hot run. For these reasons the most conclusive temperature data was obtained from temperature stabilization runs of fifteen or more seconds; by this time all inside wall temperatures and most outside temperatures had achieved a steady value.

By knowing the steady state inside and outside wall temperatures at some location, the heat flux was determined from the equation

$$q = -K \Delta T/L \tag{10}$$

where K is the conductivity of the stainless steel wall at the mean wall temperature.

VI. Results and Discussion

General

A total of one hundred nineteen test runs were made with mixture ratios varying from 0.91 to 3.57, and chamber pressures ranging from 55.2 to 150.8 psia. Ten runs (14, 20, 36, 44, 54, 55, 58, 60, 70, and 85) were not useful because the flame was blown out of the chamber when the full run pressures were started. Ten other runs (18, 51, 59, 81, and 114 to 119) were inconclusive because the hydrogen flow did not attain a steady value. This was due either to insufficient supply pressure or to leakage around a loose hydrogen injector. Further, in-accurate P_0 results were obtained for runs 1 through 43 and, therefore, the data from these runs were not used. Thus, a total of sixty valid runs were made for which complete test results could be obtained (Tables I, II, III, and IV).

Characteristic Exhaust Velocity

Theory. A digital computer was used to calculate the theoretical $C*$ and C_F. The complete details of the computer program are given in Reference 22. The results of the calculations for theoretical $C*$ as a function of mixture ratio and chamber pressure (Fig 12) showed $C*$ to be relatively in-dependent of P_c. This was the case for mixture ratios from one to three and chamber pressures from 60 to 120 psia. In fact, for mixture ratios from one to two and when the chamber pressure was increased from 60 to 120 psia, $C*$ increased less than 0.02%, and at a mixture ratio of three it increased only

0.4%. The maximum C* was found to be at a mixture ratio of approximately 2.3 for both 60 and 120 psia.

Experimental results. The experimental results of C* vs mixture ratio, r, for the spherical combustion chamber (L*44) were plotted as two curves—one for P_c of 60 psia and one for P_c of 100 psia (Fig 13). In addition, the theoretical C* curve and the results obtained by Cunningham (Ref 14) with a "full" showerhead oxygen injector are shown.

It was found that for this spherical engine the maximum C* at 60 psia was slightly higher than that at 100 psia. The mixture ratio at which maximum C* occurred for these two chamber pressures, however, was noticeably different. Maximum C* for 60 psia occurred at a mixture ratio of approximately 1.6, while for 100 psia the highest C* was obtained at a mixture ratio of approximately 2.0. A similar difference also existed in the other three engine configurations tested (Fig 14, 15, and 16).

Although the performance of the spherical chamber was quite good, the engine still exhibited, to a slight degree, a decreasing combustion efficiency with increasing mixture ratio. Values of combustion efficiency for both 60 and 100 psia varied from approximately 97% at a mixture ratio of one to 94% at a mixture ratio of about 2.2 (Table I).

The results of tests (Fig 14) on the engine with a one inch chamber extension (L* 60) showed essentially the same maximum C* at both 60 and 100 psia, with optimum performance for 100 psia again occurring at a higher mixture ratio.

Combustion efficiency was approximately 95% and decreased only slightly when the mixture ratio was increased from 1.1 to 1.9 (Table II).

When the two inch chamber extension (L*76) was used for P_c of 60 and 100 psia (Fig 15), the C* versus r curves were noticeably flatter than those of the other engine configurations tested. Runs at a P_c of 100 psia gave an optimum C* approximately 1.2% higher than at 60 psia. In addition, combustion efficiency at 100 psia decreased from 96% at a mixture ratio of one to 93% at a mixture ratio of 2.6 (Table III). Combustion efficiency at 60 psia dropped off even more rapidly at the higher mixture ratios.

The C* versus r curves for the most cylindrical combustion chamber (L*92) showed that the performance at 100 psia was noticeably higher than at 60 psia (Fig 16). Combustion efficiency at 100 psia varied from 97% at a mixture ratio of 1.2 to 95% at a mixture ratio of about 2.2 (Table IV). Further, performance for all runs was considerably higher (about 14%) than Cunningham's test results.

Effect of Engine Configuration. The curves for maximum C* at 60 and 100 psia for each engine configuration (Fig 17) were found to differ significantly from those usually obtained for cylindrical combustion chambers using liquid propellants (Ref 21:401). For liquid engines, as chamber length is reduced from optimum toward zero, cylindrical combustion chambers do not exhibit any regions of increase in performance. It must be noted, however, that L* is a somewhat abstract concept and

27

cannot be as freely used in this situation as it might be with strictly cylindrical combustion chambers. Characteristic length, L*, represents the "length" of time that injected and burning propellants are inside the combustion chamber, provided several factors are the same (Ref 1:79). Two of these factors are: the entire volume of the combustion chamber be used for the complete combustion of all oxidizer and fuel, and that there be a close similarity in all design features of the assemblies being compared. These factors were not the same in this case. The shapes varied from spherical (L*44) to practically cylindrical (L*92). Further, Nolan (Ref 6) showed that the basic flow patterns changed when the chamber was extended from the basic spherical shape. Therefore, Figure 17 is not so much a comparison of different characteristic chamber lengths as it is a comparison of different flow patterns.

In light of this, it could be concluded that with the reverse-flow engine the spherical combustion chamber offers a considerable weight advantage over the cylindrical chamber. That is, the same high level of performance was achieved in the spherical engine as in the cylindrical engine of more than twice the chamber volume. This good performance with the small chamber was probably due to the nature of the flow pattern, since the spherical shape produces the strongest vortex and also keeps the hydrogen film more intact until it reaches the front of the chamber--thus producing good mixing.

Effect of Chamber Pressure. The majority of tests were

conducted at the nominal chamber pressures of 60 and 100 psia. Three conclusions can be drawn from a comparison of the C* results of these runs.

First, the same maximum value of C* (7960 fps) and combustion efficiency (97%) were obtained for both 60 and 100 psia chamber pressures. Therefore, although these maximums occurred at different values of mixture ratio and engine configuration, it appears that maximum C* is essentially independent of chamber pressure--as predicted by theory (Fig 12).

Secondly, for the larger more cylindrical chamber configurations, the same C* performance required less volume at higher pressures (Fig 17). This effect can be explained by the results obtained from measurements of the burning velocities of gaseous hydrogen-oxygen mixtures (Ref 23:6). The burning velocity was determined for various combinations of chamber pressure and mixture ratio (see Figure 18 for these results). One of the most significant relationships apparent from these results was that the burning velocity increased as the pressure increased. Therefore, due to the fact that the burning velocity should be higher at 100 psia, less stay time (characteristic length) would be required to achieve the same C* at 100 psia as at 60 psia. Since the slightly higher performance at 60 psia over that at 100 psia for the spherical engine cannot be explained by the burning velocity effect, it can be possibly concluded that the strong vortex believed to exist with the spherical engine results in better mixing at the lower chamber pressures.

The run results (see Fig 17) further indicated that the spherical engine, which was the lightest and most compact, achieved essentially the same maximum C* performance as obtained with any other configuration. Furthermore, increasing the chamber pressure had the effect of only slightly reducing the C* performance for the spherical engine. Possibly for much higher chamber pressures the spherical engine would not offer these performance advantages.

Lastly, at the 60 psia chamber pressure the highest C* occurred at a mixture ratio of 1.6, while at 100 psia the highest C* occurred at a mixture ratio of 2.0 (Figures 13 to 16). This effect can possibly also be explained by the results of the burning velocity measurements discussed above. These results (Fig 18) indicated that when the pressure was increased from one to 14.6 atmospheres, the mixture ratio which gives maximum burning velocity increased from approximately 6.8 (70% F_2) to 8.95 (64% H_2); in addition, when the mixture ratio was increased from 1.77 (90% H_2) to 6.8, the increase in burning velocity was greater at the higher chamber pressures. Therefore, the difference in the mixture ratio required to give maximum C* at 60 and 100 psia can possibly be explained by this difference in increase of burning velocity with mixture ratio. It must be noted that for all chamber pressures the advantage of the increase in burning velocity at increased mixture ratios is countered by the disadvantage at those higher mixture ratios that the combustion efficiency decreases due to less efficient mixing of the additional oxygen.

Therefore, for a given chamber pressure and engine configuration, an optimum mixture ratio exists--below which the propellants require additional stay time due to the decrease in burning velocity, and above which the additional oxygen flow does not mix well with the hydrogen. When the mixture ratio is changed from 1.6 to 2.0 at 60 psia the effect of the increase in burning velocity is not as great as the effect at 100 psia (Fig 18). Therefore, it can be expected that the optimum mixture ratio will increase with increasing chamber pressure.

Thrust Coefficient

Theory. The theoretical thrust coefficient was calculated using the following assumptions: frozen equilibrium, ambient pressure of 14.5 psia, expansion area ratio of 1.3707, and a fifteen degree nozzle cone divergence half angle. The results showed that C_F was strongly affected by chamber pressure and only slightly dependent on mixture ratio for the range of one to three.

In fact, the plot of C_F versus P_c for a mixture ratio of 1.5 (Fig 19) gives the value of C_F to within ± 0.0020 for all other mixture ratios from one to three. That is, at $r = 1.0$ the C_F values are approximately 0.0020 higher than those for $r = 1.5$, while at $r = 3.0$ the C_F values are approximately 0.0020 lower than those for $r = 1.5$ (all at the same pressure). It was also found that as chamber pressure increased, its effect on C_F decreased due to the highly underexpanded flow.

Experimental Results. The most meaningful way to present
the experimental results (Fig 20) was in terms of the thrust
coefficient quality factor, C_{Fx}/C_{FT}, thereby combining both
the effects of mixture ratio and chamber pressure into one
term. In order to accomplish this, some interpolation between
the computed theoretical C_F values was necessary.

The values found for thrust coefficient quality factor
varied from 0.95 to 1.016, but the variation for any particu-
lar engine configuration was much less. For the engines with
L* of 44, 60, and 92 inches, the quality factor variation from
maximum to minimum value was only 0.014, 0.017, and 0.015 re-
spectively. Considering the errors in interpolating for the
C_{FT} values, this variation seems reasonable for experimental
work.

The L*76 engine was the only engine that appeared to
show a dependence of quality factor on chamber pressure. The
average value for the 60 psia runs was 0.987 while for the
100 psia runs it was 0.970. No engine configuration tested
showed any dependence of quality factor on mixture ratio.
However, there appeared to be a dependence of thrust coeffic-
ient on engine configuration. The average values of thrust
coefficient quality factors were as follows: 1.007 for the
L*60 engine, 1.001 for the L*44 engine, 0.979 for the L*76
engine, and 0.958 for the L*92 engine.

The L*60 engine gave quality factors from 0.999 to 1.016.
Although this means that C_{FT} was lower than C_{Fx}, C_{FT} is for
frozen flow and also for a fifteen degree exhaust cone half

32

angle, while the actual nozzle has a twelve degree half angle arc. Correcting C_{FT} to a twelve degree half angle cone would reduce all quality factors by approximately 0.006.

Thrust Misalignment. A slight misalignment of thrust stand components was found. This caused a variation of thrust coefficient quality factor with L* and was probably another reason why some quality factors were above one. This misalignment occurred because the engine support bars had to be slanted at different angles for various chamber extensions. This resulted in a change in engine height (the largest change was 0.2 inches and occurred between the L*60 and L*92 configurations). Thus there was a difference between the moment arm for the engine thrust and that for the calibration cable. Since the calibration procedure assumed they were the same, an error resulted. By correcting for this error, the quality factors for L*60 would be reduced approximately three per cent and all the engine average quality factors would be between approximately 0.97 and 0.95.

Engine Modifications

Oxygen Injector. The oxygen injector used in this study gave the best performance yet achieved with a reverse-flow engine. Combustion efficiencies up to 97.4% were obtained. In addition, even when the mixture ratio reached the extreme values of 0.94 (Run 57) and 3.5 (Run 119), no injector face burning or discoloration occurred.

Hydrogen Injector. While the Phase I test runs could not be used for quanitative comparison, they nonetheless did

indicate performance trends. Thus, from these results it appeared that the hydrogen injector which was chosen for use in Phase II of this study gave no increase in performance over the injector used by Cunningham. In fact, increasing the injector hole diameter from 0.041 to 0.0645 inches resulted in overheating of the chamber wall next to the hydrogen injector. Forty triangular areas of discoloration about $\frac{1}{4}$ inch long occurred on the chamber wall between the forty incoming streams of hydrogen. Although this overheating did not cause any visible damage, it can be concluded that the hydrogen injector area should have been increased by using more injection holes rather than enlarging their diameters.

Exhaust Nozzle. The insulating coating applied to the nozzle proved satisfactory since there was no burning of the converging nozzle lip. Further, the heat flux to the nozzle was reduced which resulted in less heat being picked up by the incoming hydrogen.

After approximately forty test runs, the coating started to deteriorate. Even so, after one hundred nineteen test runs, sufficient coating still remained to protect the nozzle from burning at a mixture ratio of approximately 3.5. The deterioration of the nozzle coating could have been partially due to the sequencing of the test runs. After approximately the first forty runs, the usual procedure was to run the highest temperature run of the day first. In this way the engine was cool and would be less likely damaged than if the initial engine temperature were several hundred degrees. The

disadvantage of this method was the subjection of the coating to an adverse thermal shock.

Engine Damage

Two incidents of engine damage occurred during this study. After run 16, small cracks were found in the forward hemisphere inner wall. They extended from an old thermocouple hole which had been filled. An inspection after run number 24 revealed that the cracks had progressed approximately $\frac{1}{4}$ inch further. However, since the cracks were only approximately 1/16 of an inch deep, they were successfully repaired by being stop drilled and filled with silver solder. The cracks were probably caused by thermal stresses (Appendix A).

Toward the end of the testing, it became apparent that the nozzle was "necking down". This resulted in the hydrogen injector fitting loosely between the baffle and the nozzle, and allowed hydrogen to leak out from between the injector and the nozzle. This was confirmed by an increase in the hydrogen flow for a given feedline pressure. During runs 114 to 119 the hydrogen flow increased continually during the runs rather than stabilizing. Inspection of the engine revealed extensive discoloration of both the baffle and that portion of the exhaust nozzle immediately opposite the baffle. The brass baffle was blackened, while the stainless steel nozzle had a brilliant blue-green area. Although the baffle was still useable, any further runs would have to be made with a new exhaust nozzle.

Cooling Effectiveness

Transient Temperatures. Since the chamber wall temperatures determined at three seconds were transient values, only the following general comments can be made:

1. As the nozzle insulating coating deteriorated, the chamber inner wall temperatures increased.

2. The chamber inner wall temperatures after three seconds of run were essentially independent of the chamber pressure for the range from 60 to 100 psia.

3. The forward hemisphere was hotter than the extensions or the aft hemisphere, and a typical value was 400 F when the nozzle coating was new and 650 F when the coating was deteriorated.

4. The aft hemisphere was the coolest with typical temperatures from 350 to 450 F, depending on the amount of nozzle coating remaining.

5. The largest engine (L*92) was noticeably cooler at three seconds than the other engine sizes tested. With little nozzle coating left, the forward hemisphere temperature of this engine was 70 to 100 F lower than that of the other engine sizes.

Steady Temperatures. Eight runs were made in which the recorded wall temperatures reached stable values. Due to the inability to maintain a large hydrogen flow for longer than about eight seconds, only limited success was achieved in getting a long stable run at 100 psia. Of the equilibrium temperature runs made, runs 11 and 84 were selected as

representative of the effects of chamber pressure and nozzle coating on cooling effectiveness--since they gave the minimum and maximum measured values of heat flux respectively. Run 11 was at 60 psia when the coating was new, while run 84 was at 100 psia when the coating was deteriorated. A plot of inner wall temperatures vs time for these runs is given in Figure 21.

The following comments can be made about the eight temperature stabilization runs made:

1. An increase in chamber pressure has an adverse effect on film cooling effectiveness. In one case, with all other factors (including coating condition) the same, an increase of P_c from 60 to 90 psia resulted in an increase in maximum engine temperature from 580 F to 670 F. In another case, again with all factors equal, an increase from 60 to 100 psia resulted in an increase in maximum temperature from 710 to 840 F.

2. The amount of nozzle insulation, provided by the coating, has a strong effect on equilibrium temperatures. At 100 psia, with other factors constant, the maximum temperature for a run where the coating was very thin was 840 F; while the coating was new a similar run had a 700 F maximum temperature.

3. The heat flux determined for the aft hemisphere was relatively independent of the chamber pressure and stayed within the range of 0.11 to 0.12 BTU/sec in^2.

4. The highest chamber wall heat flux for any run was always in the forward hemisphere. This heat flux was affected

GA/ME/64-8

by the chamber pressure and nozzle coating and varied from
0.11 to 0.33 BTU/sec in^2 (Runs 11 and 84 respectively).

Mass Flows

In order to accomplish the test program objectives with
a minimum amount of testing, it was important to be able to
obtain the desired mass flows for each run. The main para-
meters which affected the flow rate were the feedline pres-
sures, venturi differential pressures, and propellant tempera-
tures.

A linear relationship existed between the propellant
feedline pressure and the venturi differential pressure. This
relationship was plotted in the form of inches deflection of
recorder output for both the hydrogen and the oxygen flows
(Figures 22 and 23 respectively). Thus, in order to determine
the differential pressures and the feedline gauge pressures,
these deflections could be multiplied by their constant scale
factors. Further, by using equations (8) and (9) and correct-
ing to a reference temperature of 560 R, a mass flow was com-
puted for each value of feedline pressure. The two plots of
these values were also linear and were used in all pre-run
calculations to determine the settings of hydrogen and oxygen
control pressures which would give desired mass flows.

However, difficulties were encountered in achieving the
desired flow rates. The main difficulty was that the feedline
pressure was always lower than the control pressure set in at
the control console. Although most of this difference was
due to control pressure gauge error, which was constant and

38

predictable, some of the difference could not be predicted
and seemed to be random. For the oxygen system, this differ-
ence was above average when the oxygen supply pressure was
high. The difficulty in predicting the hydrogen flow was due
to the loosening of the injector. As the testing progressed,
there was a trend toward higher mass flow for the same control
pressure (Fig 21).

The prediction of the propellant feedline temperatures
also presented problems which affected the ability to achieve
the desired mass flows. The hydrogen temperature was usually
close to the ambient temperature. The oxygen temperature,
however, was not easily predicted. It was always lower than
ambient and was much lower when the oxygen supply pressure was
high.

VII. Conclusions

1. The same maximum value of C* (7960 fps) and combustion efficiency (97%) were obtained for both 60 and 100 psia chamber pressures. Therefore, although these maximums occurred at different mixture ratios and for different engine configurations, it appears that maximum C* was essentially independent of chamber pressure--as predicted by theory.

2. The optimum C* occurred at higher mixture ratios for higher chamber pressures. With the injector used in this study, maximum C* at a chamber pressure of 60 psia occurred at a mixture ratio of 1.6, while at 100 psia it occurred at 2.0.

3. The spherical combustion chamber, which was the smallest, achieved essentially the same maximum C* performance as obtained with any of the longer configurations. Further, the spherical chamber gave better performance than two of the engines with larger chamber volume. This advantage decreased with increasing chamber pressure, but was still present at 100 psia. Therefore, it appears that the best combustion chamber shape was spherical.

4. To obtain a certain level of combustion efficiency in the nearly cylindrically shaped combustion chambers, L*76 and L*92, a larger chamber volume was required at 60 psia than at 100 psia.

5. The heat flux and wall temperatures increased as the chamber pressure was increased.

6. For a chamber pressure of 100 psia, the equilibrium wall temperatures were never greater than 900 F; therefore, the engine should be capable of continuous operation at 100 psia.

7. The insulating coating applied to the exhaust nozzle was very effective in reducing the heat flux through the nozzle. This kept the hydrogen injection temperature low and resulted in less heat flux to the engine walls and lower wall temperatures. The coating was also effective in protecting the convergent section of the nozzle from the erosion burning that had occurred in previous studies.

8. The modified showerhead oxygen injector used in this study gave better performance than the showerhead, impinging stream, and swirl type injectors used previously.

VIII. Recommendations

In the event that further studies are undertaken with this type of rocket engine, the following recommendations are made:

1. A smaller nozzle throat area should be used if further studies are to be made with the same propellant supply system and at chamber pressures above 100 psia. This would allow higher levels of stable hydrogen flow and higher obtainable chamber pressures. Further, the lower flow rates necessary to achieve a certain chamber pressure would enable more testing time before depleting the propellant supply. In addition, a smaller spherical engine should be used so as to keep L* near 40 inches.

2. It is possible that higher combustion efficiency or lower optimum L* could be achieved by using an oxygen injection velocity less than sonic. This should increase the stay time of the oxygen and allow more time for it to mix with the hydrogen.

3. The exhaust nozzle and hydrogen injector should be made of one piece and should be made of the same material as the baffle. This should eliminate the problem of the nozzle necking down and allowing hydrogen to flow between the injector and the nozzle. Further, for test purposes, if the nozzle and injector were made of iron, they would have a higher thermal conductivity than the stainless steel now used. This would reduce the temperature of the nozzle convergent section.

4. Since the thick stainless steel walls caused such high thermal stresses (Appendix A), it may be better to use either thinner chamber walls or a metal with a higher thermal conductivity.

References

1. Herrick, J. W. Rocket Encyclopedia. Los Angeles: Aero Publishers, 1959.

2. Auble, C. M. "A Study of Injection Processes for Liquid Oxygen and Gaseous Hydrogen in a 200-Pound-Thrust Rocket Engine." NACA RM #56I25a, (January 1957).

3. Keating, D. A. and Roundy, R. W. "Closed Ecology." WADD TR 61-129, (March 1961).

4. Guarino, N. J. An Experimental Study of Airflow Injected Tangentially into a 2-Dimensional Chamber of Circular Shape. Unpublished Thesis. Institute of Technology (AU), Wright-Patterson AFB, Ohio (August 1958).

5. Morton, L. C. The Design and Testing of a Small Rocket Motor of 50 Pounds Thrust, Utilizing Reversed-Flow Cooling with Gaseous Hydrogen and Oxygen as Propellant Combination. Unpublished Thesis. Institute of Technology (AU), Wright-Patterson AFB, Ohio (September 1959).

6. Nolan, L. S. An Interferometer Study of Reverse-Flow in a 2-Dimensional Chamber. Unpublished Thesis. Institute of Technology (AU), Wright-Patterson AFB, Ohio (August 1960).

7. James, R. N. An Evaluation of a Reverse-Flow Film-Cooled Rocket Engine. Unpublished Thesis. Institute of Technology (AU), Wright-Patterson AFB, Ohio (August 1960).

8. Keller, R. G., Macko, R. F., and Pickitt, J. L. Operations Manual for the Rocket Engine Test Facility of the Department of Mechanical Engineering. Air Force Institute of Technology. Wright-Patterson AFB, Ohio (August 1961).

9. Macko, R. F. Rocket Engine Performance with Reversed-Flow Cooling II. Unpublished Thesis. Institute of Technology (AU), Wright-Patterson AFB, Ohio (August 1961).

10. Johnston, J. R. The Effect of Increasing Characteristic Chamber Length in Combination with Various Oxygen Injectors on the Performance of a Reversed-Flow Film-Cooled Rocket Engine. Unpublished Thesis. Institute of Technology (AU), Wright-Patterson AFB, Ohio (August 1963).

11. Krumpe, R. H. Experimental Evaluation of a Small Rocket Engine, Utilizing Reverse-Flow Cooling with Gaseous Hydrogen and Oxygen as Propellants Injected with a Swirling Component. Unpublished Thesis. Institute of Technology (AU), Wright-Patterson AFB, Ohio (August 1960).

GA/ME/64-8

12. Keller, R. G. _Performance Evaluation of a Gaseous Hydrogen-Oxygen Rocket Engine Using Propellant Swirl Injectors_. Unpublished Thesis. Institute of Technology (AU), Wright-Patterson AFB, Ohio (1961).

13. Kineer, B. L. _Performance of a Small Rocket Engine with Different Propellant Injection Angles and Chamber Lengths_. Unpublished Thesis. Institute of Technology (AU), Wright-Patterson AFB, Ohio (August 1962).

14. Cunningham, J. W. _Performance Evaluation of a Gaseous Hydrogen-Oxygen Rocket Engine Using Different Oxygen Injectors and Chamber Lengths_. Unpublished Thesis. Institute of Technology (AU), Wright-Patterson AFB, Ohio (August 1963).

15. Heye, J. F. _Performance Evaluation of Reverse-Flow Cooling Combustion Chamber_. Unpublished Thesis. Institute of Technology (AU), Wright-Patterson AFB, Ohio (August 1960).

16. Agosta, J. J. _The Effect of Chamber Length and Mixture Ratio on Combustion Performance of a Small Combustion Chamber Utilizing Reverse-Flow Cooling_. Unpublished Thesis. Institute of Technology (AU), Wright-Patterson AFB, Ohio (August 1961).

17. Ow, G. Y. W. _An Evaluation of Film Cooled Gaseous Hydrogen and Oxygen Rocket Engine of 100 Pounds Thrust_. Unpublished Thesis. Institute of Technology (AU), Wright-Patterson AFB, Ohio (August 1960).

18. Pickitt, J. L. _Design of, and Proposed Test Program for, a Film-Cooled Nozzle_. Unpublished Thesis. Institute of Technology (AU), Wright-Patterson AFB, Ohio (August 1961).

19. Alser, D. J. _An Experimental Investigation of Nozzle Cooling for a Small Rocket Engine_. Unpublished Thesis. Institute of Technology (AU), Wright-Patterson AFB, Ohio (August 1963).

20. Sutton, G. P. _Rocket Propulsion Elements_ (Third Edition). New York: John Wiley and Sons Inc., 1963.

21. Barrere, M., Jaumotte, A., Deveubeke, B., and Vanderkerckhove, J. _Rocket Propulsion_. New York: Elsevier Publishing Company, 1960.

22. Anderson, F. E. _Analytical Investigation of Rocket Engine Performance Degradation due to the Presence of an Inert Diluent_. Unpublished Thesis. Institute of Technology (AU), Wright-Patterson AFB, Ohio (June 1964).

23. Bollinger, L. E. and Edse, R. "Research on a Premixed Gaseous Rocket Propellant." WADD TN 55-388, (August 1955).

24. Haven, G. B. The Design of Steam Boilers and Pressure Vessels (Second Edition). New York: John Wiley and Sons, Inc., 1923.

25. Faires, V. M. Design of Machine Elements (Third Edition). New York: The Macmillan Company, 1957.

26. Timoshenko, S. and Goodier, J. N. Theory of Elasticity (Second Edition). New York: McGraw-Hill Book Company, Inc., 1951.

27. Baumeister, T. Marks' Mechanical Engineers' Handbook (Sixth Edition). New York: McGraw-Hill Book Company, Inc., 1958.

28. Machine Design. The Seals Book (1961 Edition). Cleveland: The Penton Publishing Company, 1961.

29. Stearns, R. F., Jackson, R. M., Johnson, R. R., Lanson, C. A. Flow Measurement with Orifice Meters. New York: D. Van Nostrand Company, Inc., 1951.

30. Binder, R. C. Fluid Mechanics (Second Edition). New York: Prentice-Hall, Inc., 1949.

31. Shapiro, A. H. The Dynamics and Thermodynamics of Compressible Fluid Flow (Volume 1). New York: The Ronald Press Company, 1953.

32. Keenan, J. H. and Kaye, J. Gas Tables. New York: John Wiley and Sons, Inc., 1949.

Appendix A

Combustion Chamber Stress Calculations

A basic engine consisting of two hemispheres and two
chamber extensions was available at the beginning of this
study. These sections were all $\frac{1}{4}$ inch thick and made of AISI
type 304 stainless steel. Although intuitively the $\frac{1}{4}$ inch
walls seemed quite adequate to withstand the maximum antici-
pated chamber pressure of roughly 300 psia, it was decided to
verify this analytically.

Determination of the stress due to chamber pressure was
greatly simplified by using the stress equation for a thin-
walled pressure vessel. Haven (Ref 24:51) stated that this
equation results in an error of 6/10 of one per cent if the
wall thickness is not more than ten per cent of the internal
radius; and not more than two per cent when the internal pres-
sure does not exceed 1/3 of the allowable fiber stress. Since
this engine wall thickness was 12.5% of the internal radius
and the maximum internal pressure was 300 psia, the equation
was sufficiently accurate. Therefore, for the more critical
case of the cylindrical portion of the chamber, the tensile
strength required of the walls was calculated to be

$$S = PR/2L \qquad\qquad \text{(Ref 25:156)} \qquad (11)$$

$$= (300)(4)/(2)(1/4) = 2400 \text{ psi}$$

Thermal stresses were also present. This was due to the
high temperature drop across the engine walls caused by the
low thermal conductivity of stainless steel. An approximation

of the value of this stress was made from the case of steady heat flow through a long, thin-walled cylinder. The largest stress occurred at the inner and outer surfaces and was calculated from

$$\sigma = \propto E \, \Delta T/2(1-\gamma) \qquad \text{(Ref 26:414)} \qquad (12)$$

where, at 1000 F inner wall temperature:

$$\propto = 10.02 \times 10^{-6} \text{ in/in F} \qquad \text{(Ref 20:99)}$$

$$E = 22.2 \times 10^6 \text{ psi} \qquad \text{(Ref 20:98)}$$

$$\gamma = 0.305 \qquad \text{(Ref 27:5-6)}$$

hence $\sigma = 160 \, \Delta T$ \qquad (13)

From similar calculations, the thermal stress for a 1400 F inner wall temperature was found to be 140 (ΔT). Temperature measurements indicated that if the inner wall temperature reached 1000 F, a 300 degree temperature drop across the wall could be expected. This would give a thermal stress approaching 48,000 psi.

From these calculations it was concluded that thermal stresses are of far more importance than the stresses due to chamber pressure. Therefore, the safe limit of engine operation was determined by the wall temperatures rather than chamber pressure. Further, it was assumed that if the forward hemisphere inner wall reached 1000 F, then the thermal stress would exceed the yield strength of 17,000 psi, but not the ultimate tensile strength of 65,000 psi (Ref 20:98).

GA/ME/64-8

Appendix B

Combustion Chamber Seals and Bolts

Since a pressure check of the assembled engine revealed
significant leakage from between the hemispheres and chamber
extensions, it was necessary to modify the engine seals. The
previously used flat copper seals had a surface area of approx-
imately 9.6 in^2. Since each joint is held together with
twelve $\frac{1}{4}$-inch bolts, and the recommended seating stress for a
1/8-inch thick copper seal is 36,000 psia (Ref 28:107), it
became obvious that the surface area was too large to allow
proper seating.

Although a plain corrugated metal gasket was well suited
for this application (Ref 28:105), it was decided to continue
using flat copper seals due to their immediate availability.
It should be noted that if flat copper seals had continued to
be unsuccessful, aluminum seals might have been used since
they have a higher temperature limit and a lower recommended
seating stress (Ref 28:107).

By reducing the area of the copper seal to 1.1 in^2 a
successful seal was obtained (Fig 3). A pressure check to
450 psig revealed no leakage with the exception of a slight
leakage around the engine thermocouples. Attempts to stop
these leaks were not successful, but the amount of leakage was
small and was considered tolerable.

In order to insure proper seating of the engine seals;
high temperature, high strength bolts were obtained. Further,

the bolts used previously had become severely corroded and were difficult to install. The new bolts conformed to AMS 5735 and were designed for use when high strength at temperatures as high as 1300 F is required and oxidation resistance up to 1500 F is desired. They can also sustain 65,000 psi at 1200 F for 23 hours.

Appendix C

Injector Hole Design

The mass flow through an orifice with critical flow
pressure at the throat can be found from

$$\dot{m} = C_d A P_s \left[\frac{gk}{\mu_s R T_s} \left(\frac{2}{k+1}\right)^{\frac{k+1}{k-1}} \right]^{\frac{1}{2}} \qquad \text{(Ref 27:4-61)} \qquad (14)$$

where μ_s is the gas law deviation factor (Ref 29:56). Since
C_d should be between 0.95 and 0.99 for a fairly long circular
tube (Ref 30:129) and μ_s would be slightly greater than 1
(Ref 29:56), both of these parameters can be approximated to
be unity. This makes the value to be calculated for the area
slightly smaller than the maximum injection area that would
allow choked flow; therefore, the injection velocity would
still be sonic. With these simplifications, the equation can
be rearranged to give an expression for the injection area re-
quired for sonic injection.

$$A = \frac{(\dot{m}/P_s g)(gkRT)^{\frac{1}{2}}}{k \left[\left(\frac{2}{k+1}\right)^{\frac{k+1}{k-1}} \right]^{\frac{1}{2}}} \qquad \text{(Ref 20:50)} \qquad (15)$$

Using the above equation, the following steps are taken
to calculate the injection area of each injector:

1. Assume a value of propellant inlet temperature, T_s.
This determines the value of k.

2. Estimate the value of C* that can be expected for the critical run condition. It can be shown (Ref 14:31, 32) that if the flow is choked for the run condition that requires the lowest mass flow then the flow will be choked for all higher mass flows at the same mixture ratio. Therefore, the run condition used for the oxygen design was 60 psia at a mixture ratio of one, and for hydrogen it was 60 psia at a mixture ratio of three.

3. Calculate the mass flow at the critical run condition.

4. Calculate the minimum value of P_s that will give choked flow for the critical run condition from

$$P_s = \frac{P_c}{\left(\frac{2}{k+1}\right)^{k/(k-1)}} \qquad \text{(Ref 31:84)} \qquad (16)$$

For a chamber pressure of 60 psia and a k of 1.4:

$P_s = (60)/(0.5283) = 114$ psia

5. Calculate injection area, A.

6. Determine the number of injection holes and their diameters.

Oxygen Injector

1. Since the oxygen feedlines and manifold are relatively cool during engine operation, assume $T_s = 500$ R. Therefore, k= 1.397 (Ref 32:107).

2. For $P_c = 60$ psia and r = 1.0, estimate C* to be 7730 fps (Ref 14).

GA/ME/64-8

3. $\quad \dot{m}_p = (A_t g) P_c / C*$ \hfill (1)

$\quad\quad = (25.63)(60)/(7730) = 0.194 \text{ lbm/sec}$

$\quad \dot{m}_0 = \dot{m}_p/(1+1/r)$ \hfill (17)

$\quad\quad = (0.194)/(2) = 0.097 \text{ lbm/sec}$

4. Since k is approximately 1.4, use $P_s = 114$ psia.

5.

$$A_0 = \frac{(\dot{m}_0/P_s g)(gkRT_0)^{\frac{1}{2}}}{k\left[\left(\frac{2}{k+1}\right)\frac{k+1}{K-1}\right]^{\frac{1}{2}}}$$ \hfill (18)

$$= \frac{0.097/(114)(32.2)(1041.8)}{0.8102} = 0.034 \text{ in}^2$$

6. Use the same small hole diameter as used in Cunningham's showerhead injector, 0.036 inches. Therefore:

$\text{Number of oxygen injection holes} = 4A_0/\pi D_0^2$ \hfill (19)

$\quad\quad\quad\quad\quad\quad = 4(0.034)/\pi (0.036)^2$

$\quad\quad\quad\quad\quad\quad = 33$

The final design was selected to have thirty-two holes of 0.036 inch diameter.

Hydrogen Injector

1. Since the hydrogen is heated by the exhaust nozzle before injection, estimate the inlet temperature to be 240 F. Therefore, k = 1.399 (Ref 32:122).

2. For $P_c = 60$ psia and r = 3.0, estimate C* to be 7400 fps (Ref 14).

3. $\dot{m}_p = (A_t g) P_c / C*$ (1)

      $= (25.63)(60)/(7400) = 0.206 \text{ lbm/sec}$

    $\dot{m}_H = \dot{m}_p / (1+r)$ (20)

      $= (0.206)/(4) = 0.051 \text{ lbm/sec}$

4. Since k is approximately 1.4, use $P_s = 114$ psia.

5.
$$A_H = \frac{(\dot{m}_H / P_s g)(gkRT_H)^{\frac{1}{2}}}{k \left[\left(\frac{2}{k+1} \right) \frac{k+1}{k-1} \right]^{\frac{1}{2}}}$$
          (21)

$$= \frac{0.051/(114)(32.2)(4915)}{0.8102} = 0.085 \text{ in}^2$$

6. Use the same number of injection holes (forty) used previously by Krumpe and Cunningham. Therefore:

$$D_H = (4A_H / 40\pi)^{\frac{1}{2}}$$
          (22)
$$= (0.085/10\pi)^{\frac{1}{2}} = 0.052 \text{ inches}$$

The final design was selected to have forty holes of 0.0645 inch diameter (Fig 7). The decision to use a larger injector hole diameter was based on the high feedline pressure required before (Ref 14:31) to obtain a flow rate of 0.6 lbm/sec. From these previous results, it was determined that unless the diameter was larger than .052 inches, the required feedline pressure for this study would exceed 1000 psia at the higher chamber pressure runs. Therefore, it was finally decided to

use a diameter of 0.645 inches which was 0.012 inches larger than the value calculated above. Depending on C_d, this larger diameter might make the injection velocity less than sonic for the lower chamber pressure runs; however, no problems or effect on C* had been encountered when this same injection area had been used before (Ref 11).

Appendix D

Run Checklist (as revised from Ref 8:44)

11. Fill ice bath--2 required

 1. Green light, all clear--on

 2. Check all gauges for zero pressure

 3. Zero all loaders

 4. N control pressure--bleed valves--closed (Turn cw)

 5. Amber light, stand by--on

 6. All other switches on console--off

 7. Master relay power--on (Switch located under console)

 8. Master power--on (Turns on console lights, 110 VAC circuit, and activates master power relays)

12. a. Open large door
     b. Connect engine thrust, chamber pressure, ignition wires, and thermocouples

14. Engine supply valves--6 closed

16. Open required number H, O, N bottles--record

17. a. H, O, N supply pressure gauges--record "before" pressures
     b. Record cell temperature

23. Engine supply valves--2 open, 4 closed (Listen for leakage)

22. Turn on intercom

 9. a. Recorder--on
     b. Recorder light on

13. a. Record atmospheric pressure and temperature
     b. Turn on 10 VDC power
     c. Calculate run pressure settings
     d. Center all recorder dots to line desired
     e. Block off temperature channels not being used
     f. Run recorder, check for line static

18.   a. Align engine for no binding of H_2 supply lines
     b. Adjust spark gap of ignition wires
     c. Calibrate thrust

21.   a. Check engine
     b. Close cell door

27. DC power--on

DO THE FOLLOWING IN FAST SEQUENCE

31. Auto purge ready--on (Connects preset temperature limit devices into circuit)

32. Standard purge ready--on (Activates warning bell in cell, initiates 60 sec thermal delay)

33. Water purge ready--on (Energizes solenoid which supplies 15 psig air to water valve to hold i. closed)

35. Critical power--on (Power to #3, 4, 5 solenoids, and ignition ready. Therefore, O and H domes directly connected to start pressure.)

37. Large water purge valve--open, turn up (Need water purge switch on, 110 VAC power, and 15 psig air supply to prevent cell flooding)

40. Control room lights--off (Optional)

44. N control pressure shut-off--open (CCW)

45. Zero engine run timer

SEMI-CRITICAL PERIOD

34. Red lights, warning--on

47. Check for green lights then: Set purge pressure ___PSIG (Approximately 150 psig)

48. Set H run pressure ____PSIG

49. Set O run pressure ____PSIG

51. Timing light--on

CRITICAL PERIOD

53. Recorder--on (Check 10 VDC and "dots")

55. H start pressure to approximately 15 PSIG

56. Ignition--on (Pulse self return switch for $\frac{1}{2}$ sec maximum)

57. Increase O start pressure to shift flame front into chamber (Usually hear "pop")

59. H-O run pressure--on (This energizes solenoids 1 and 2 and starts run timer). Run for at least 3 sec

60. Purge--on, 2 sec is sufficient (Releases all solenoids to power off)

61. Purge stop--on (Puts power to #5 solenoid, cutting off N purge)

64. Recorder--off

63. a. H and O start pressure loaders--zero
    b. Insure that all flow has stopped

PRIMARY SHUT DOWN

73. Red lights, warning--off

79. Record engine run time (Zero timer)

80. Record H, O, N "after" pressures

67. N purge pressure loader--zero

69. Purge stop--off

70. Purge--off

71. H-O run pressure switch--off (Initiates 60 sec thermal delay)

SECONDARY SHUT DOWN (If no further runs are to be made)

76. Turn water purge valve--off, down 90°

66. H and O run pressure--zero

27. DC power off

72. Critical power--off

77. Water purge ready--off (Water valve must be off)

74. Standard purge ready--off

75. Auto purge ready--off

LIST OF FIGURES

GA/ME/64-S

FIGURE I.   ENGINE ASSEMBLY (FULL SCALE)

Figure 2

Engine Assembly Parts List

No.	#/Assembly	Item	Designer	Figure
1	1	Forward Hemisphere	Morton	Ref 13:106
2	1	Aft Hemisphere	Krumpe	Ref 13:105
3	0 to 2	Chamber Extension	Kineer	Ref 14:11
4	1	Hydrogen Manifold	Keller	Ref 13:43
5	1	Baffle	Keller	Ref 13:44
6	1	Hydrogen Injector	Keller	Figure 7
7	1	Nozzle	Keller	Ref 14:14
8	1	Oxygen Injector	Vaughan	Figure 5
9	1	Oxygen Spacer	Cunningham	Ref 14:18
10	1	Oxygen Head	Morton	Ref 7:55
11	1 to 3	Seal, Hemisphere	Vaughan	Figure 3

No.	#/Assembly	Item	Part Number	Size-Thread
12	12	Bolt, Oxygen Head	MS9033-10	.190(#10)-32
13	None or 12	Bolt, Hemisphere, Short	MS9034-14	.250-28
14	None or 12	Bolt, Hemisphere, Long	MS9034-28	.250-28
15	12	Bolt, Hydrogen Manifold	MS9035-29	.3125-24
16	8	Bolt, Nozzle	MS9033-05	.190(#10)-32
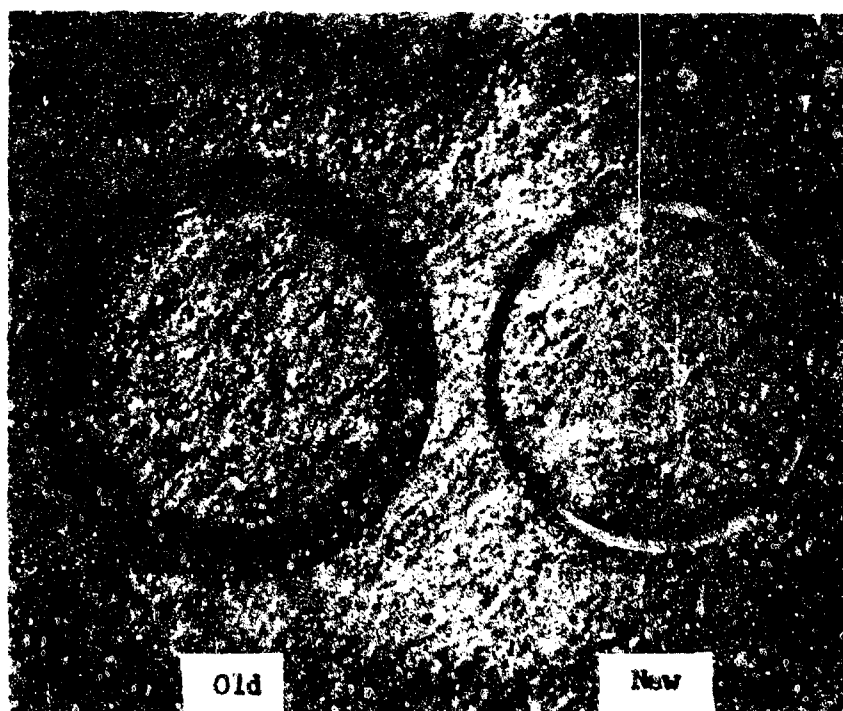
Figure 3. Old and New Engine Seals

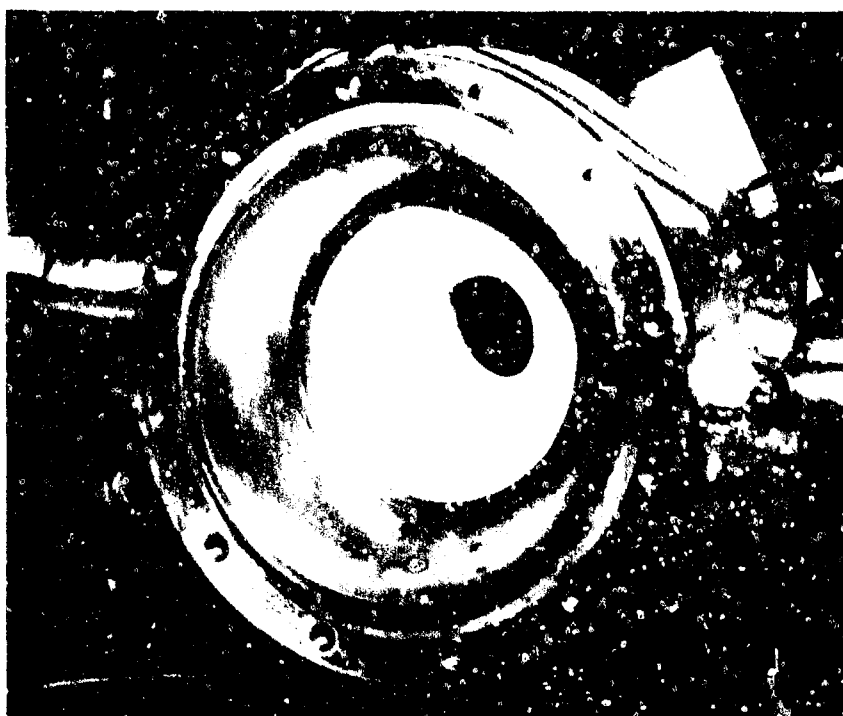
Figure 4. Coated Exhaust Nozzle (Convergent Section)
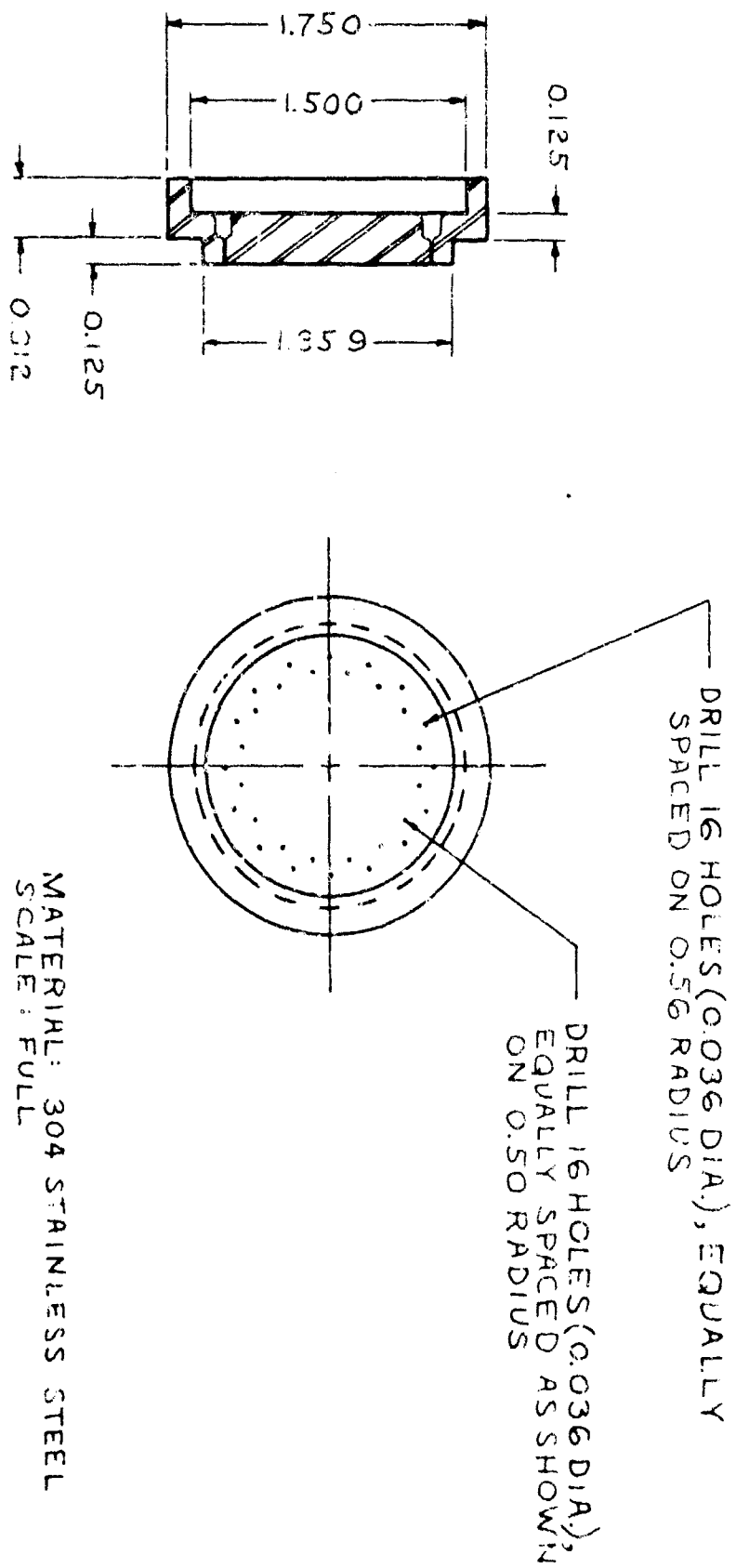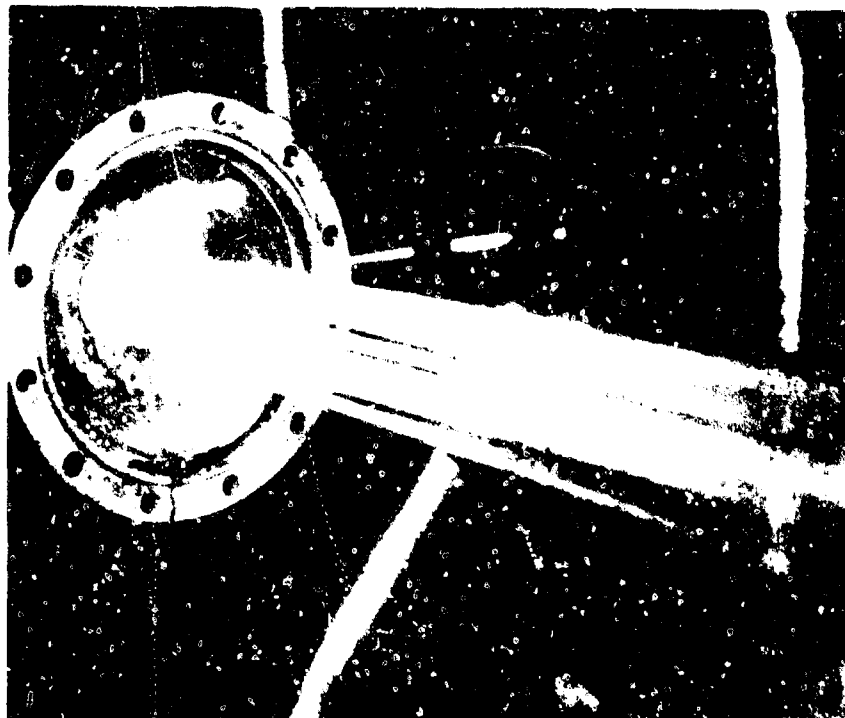As Seen from Inside of Engine

FIGURE 5. NEW OXYGEN INJECTOR

1.750

1.500

0.125

0.125

0.312

1.359

DRILL 16 HOLES (0.036 DIA.), EQUALLY SPACED ON 0.56 RADIUS

DRILL 16 HOLES (0.036 DIA.), EQUALLY SPACED AS SHOWN ON 0.50 RADIUS

MATERIAL: 304 STAINLESS STEEL
SCALE: FULL

Figure 6. New Oxygen Injector Water Spray Pattern
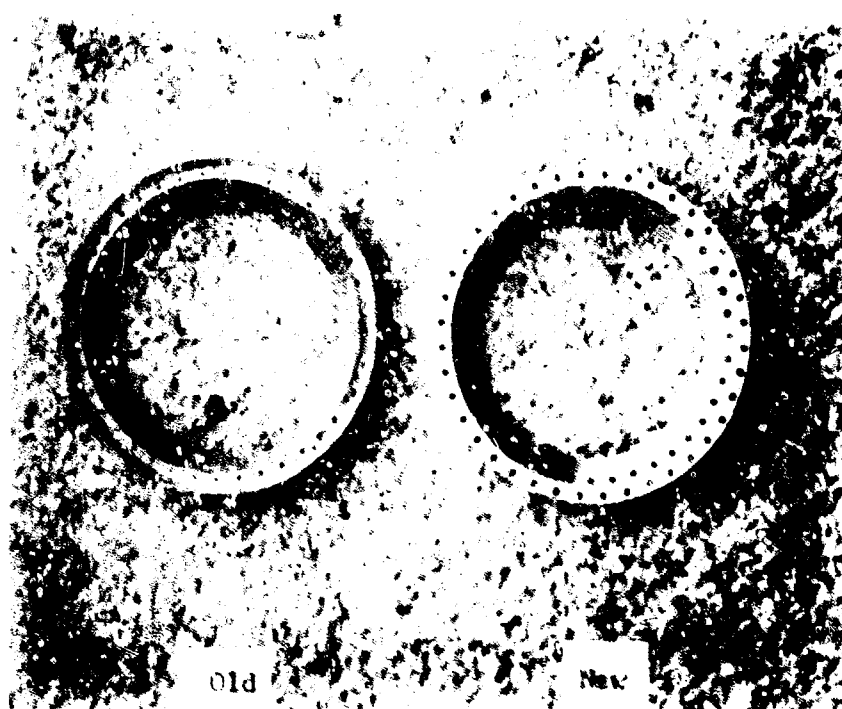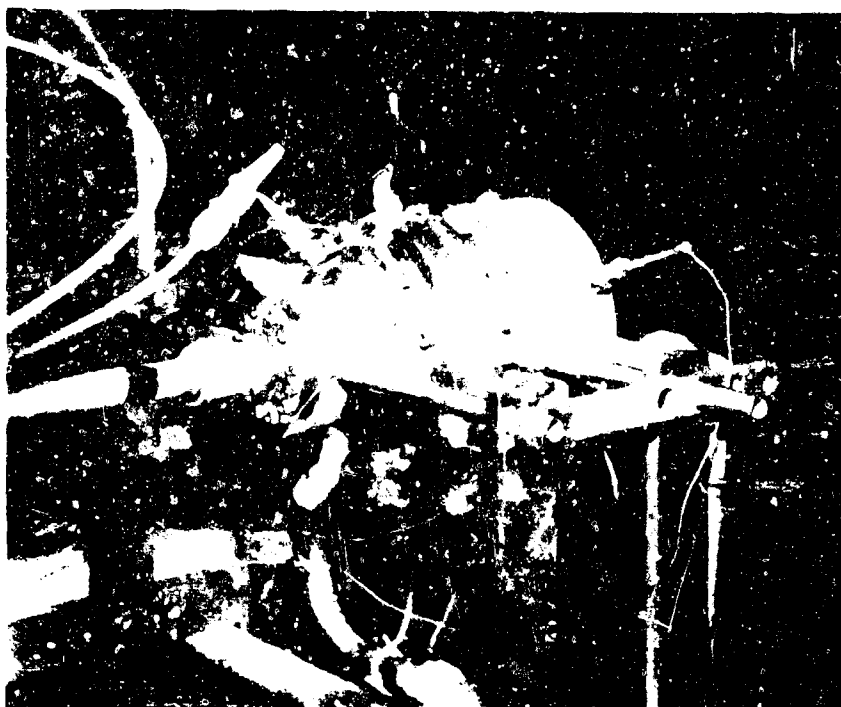

Figure 7. Old and New Hydrogen Injectors
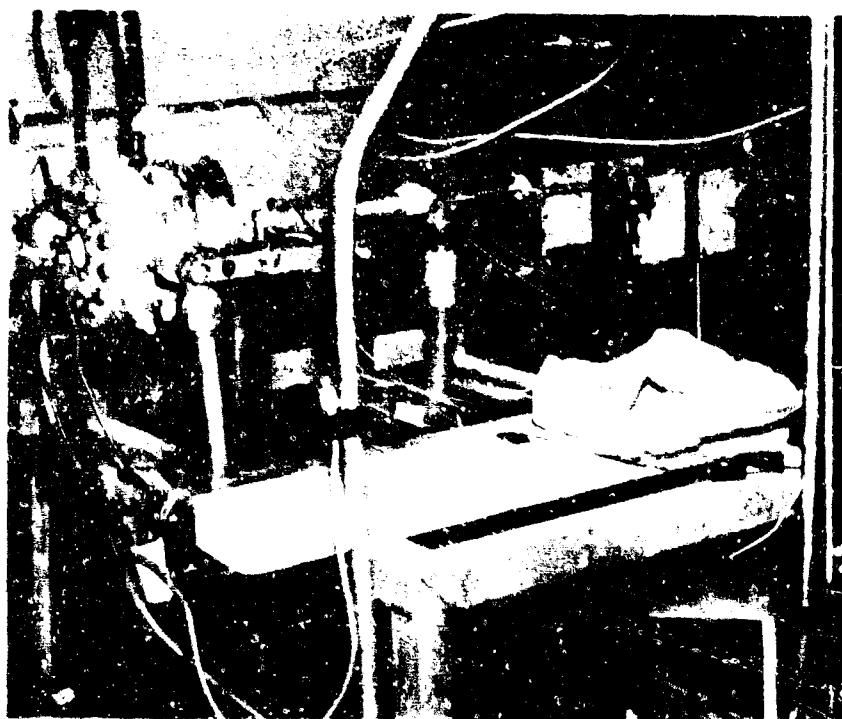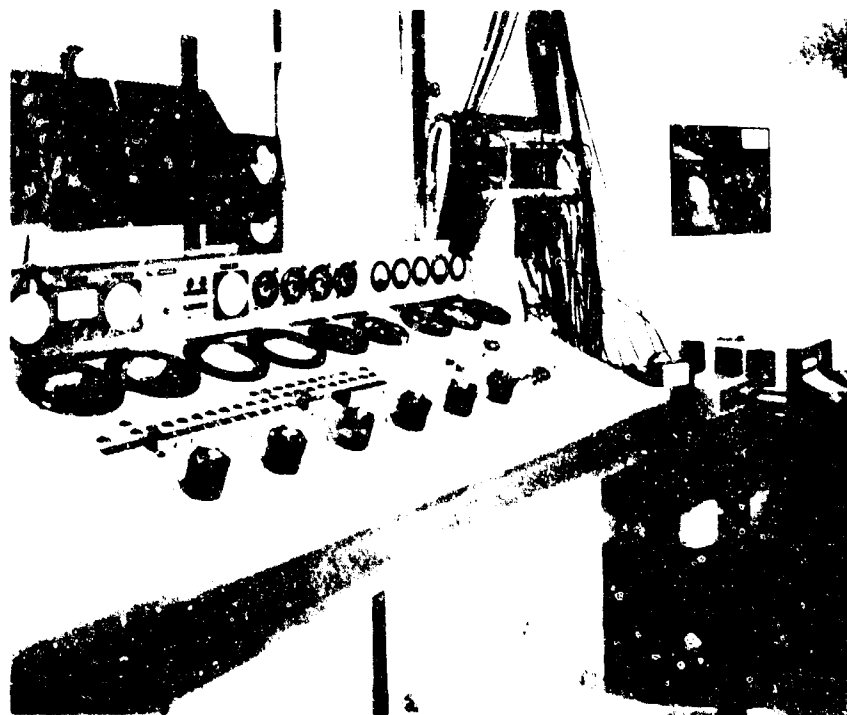
Figure 8a,b. Assembled Engine and Test Stand
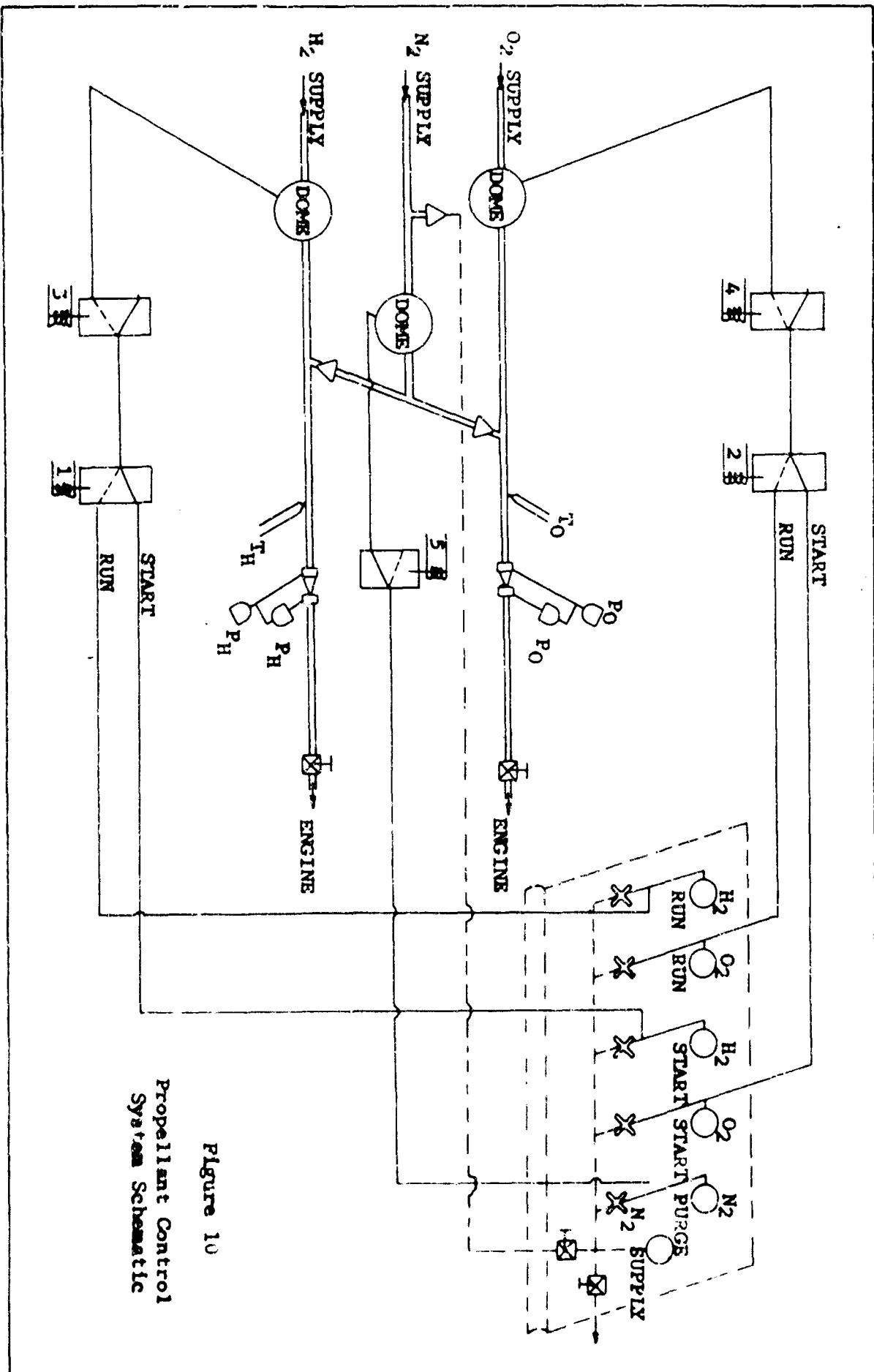
Figure 9. Control Room

Figure 10
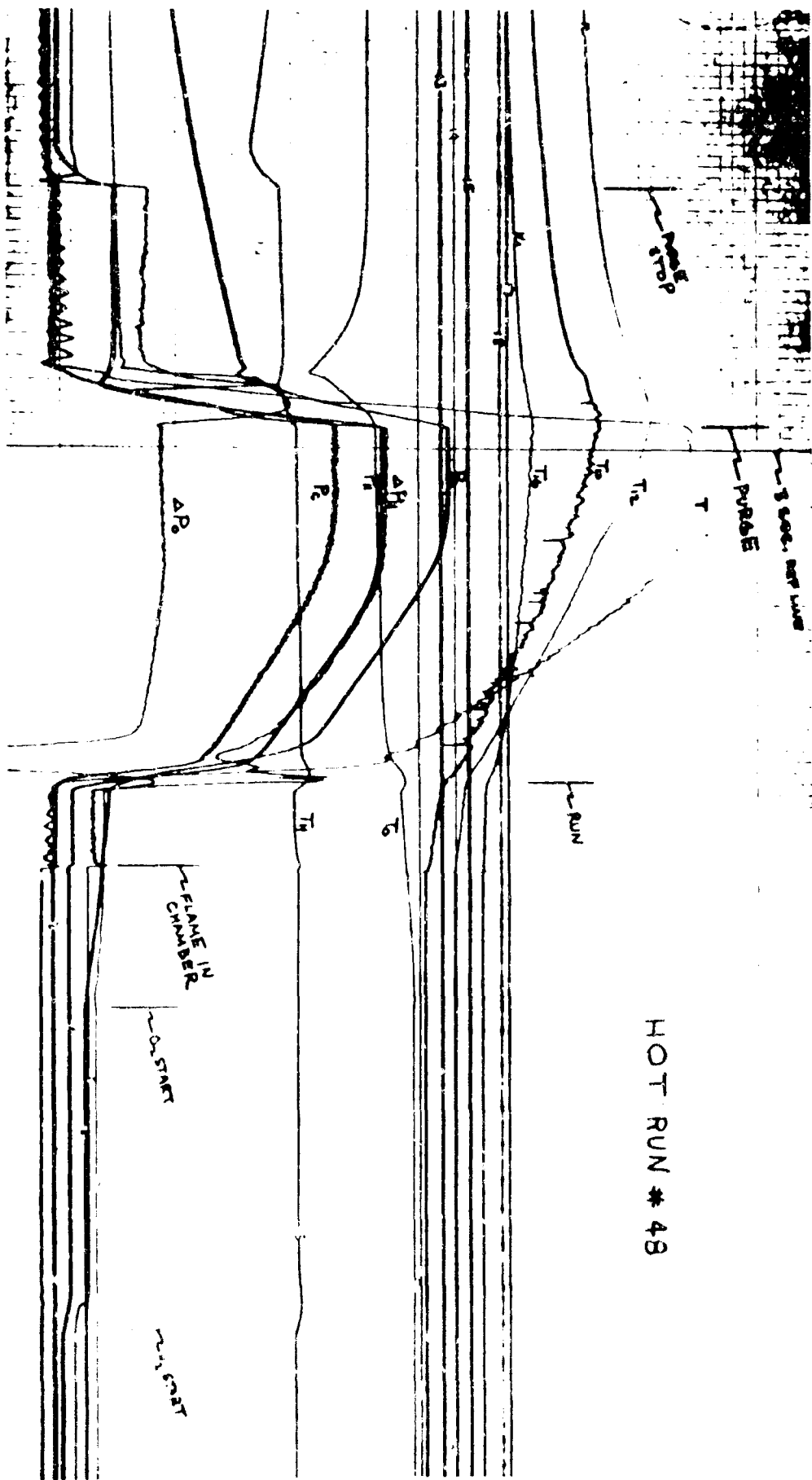Propellant Control
System Schematic
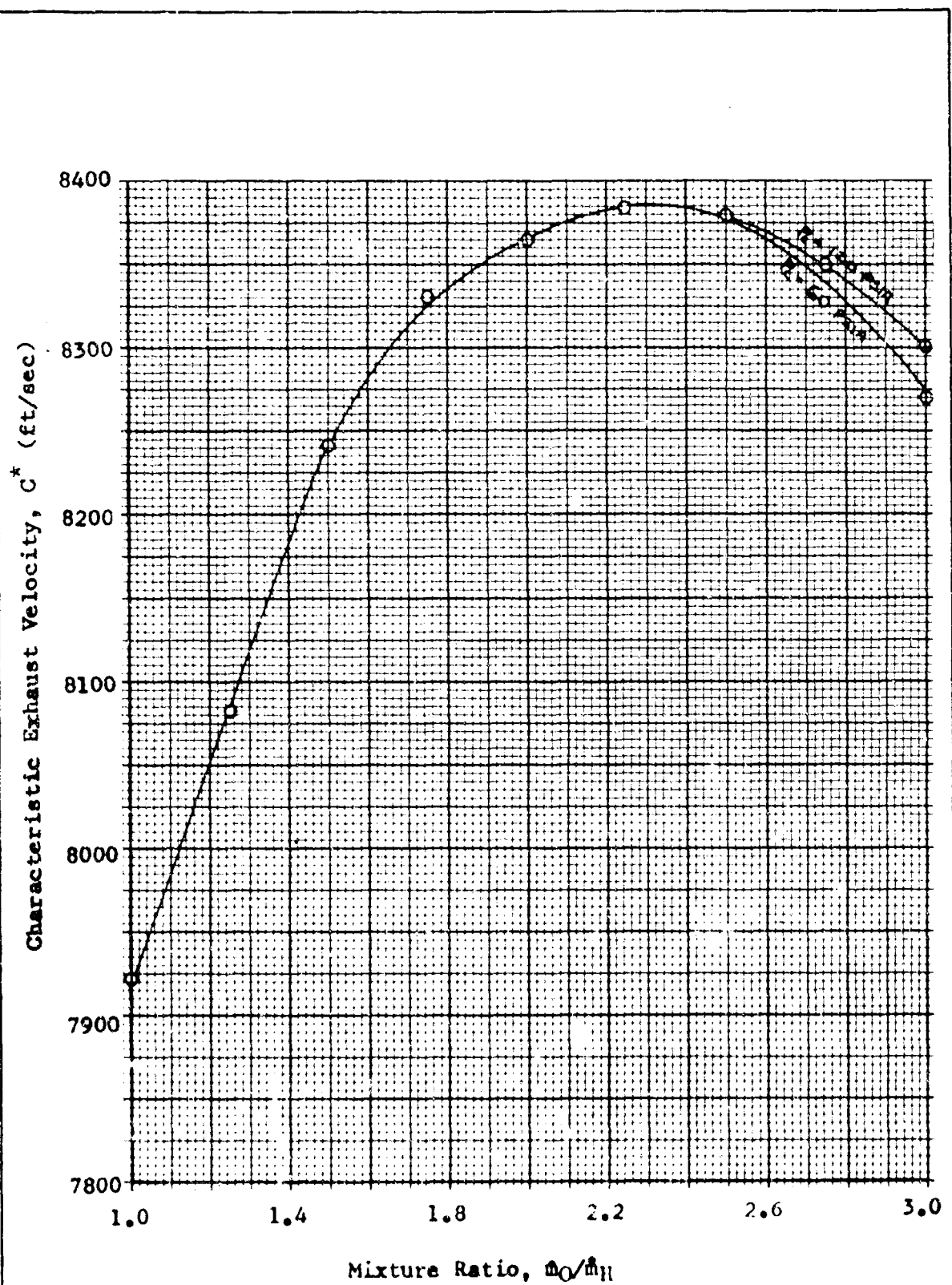
Figure 11. Sample Recorder Output Sheet

Figure 12

Theoretical C^* vs Mixture Ratio
for Gaseous H_2-O_2

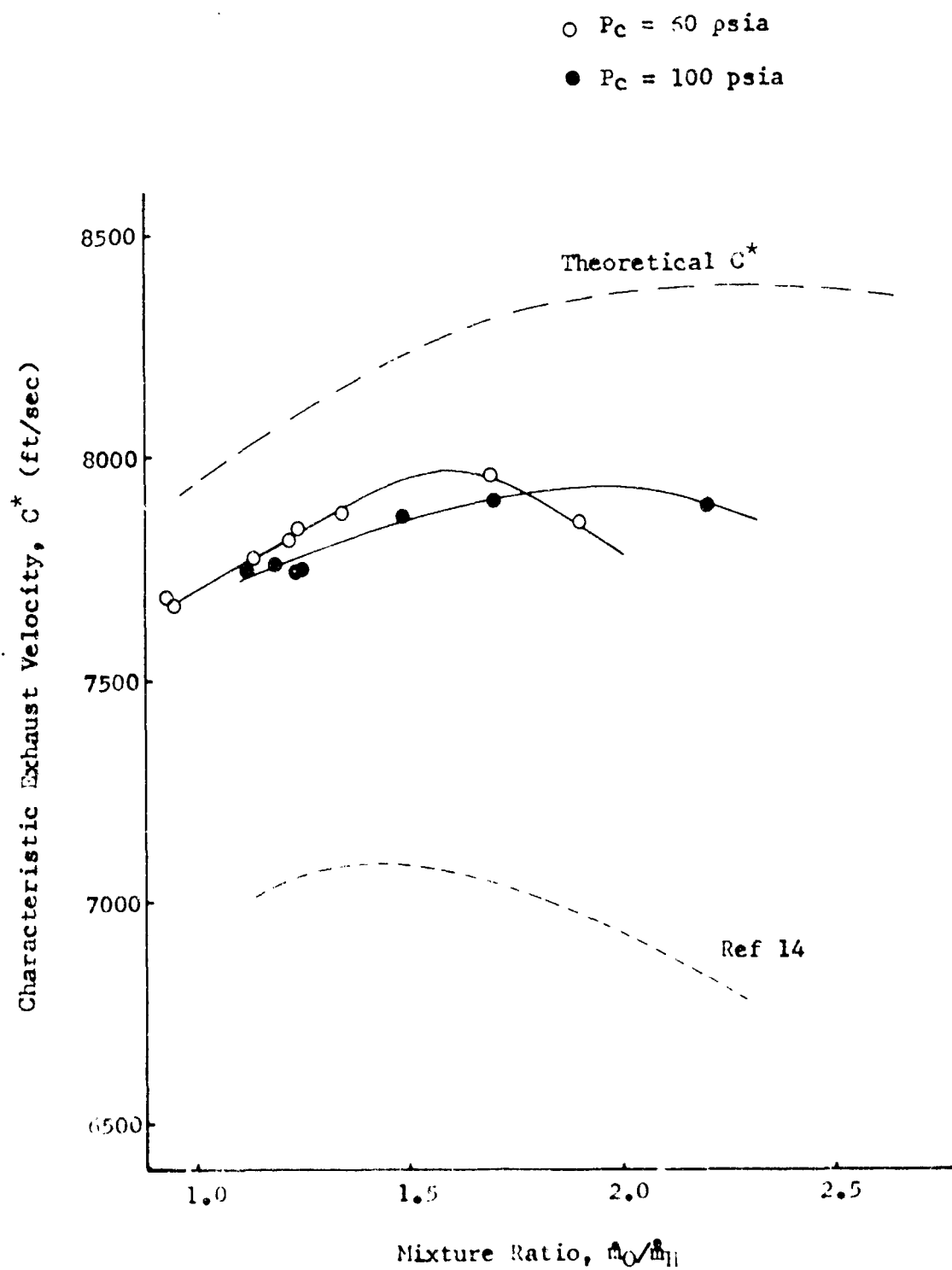Figure 13

The Effect of Chamber Pressure on C^*
for the L^*44 (Spherical) Engine

Figure 14

The Effect of Chamber Pressure on C^*
for the L^*60 (One Inch Extension) Engine
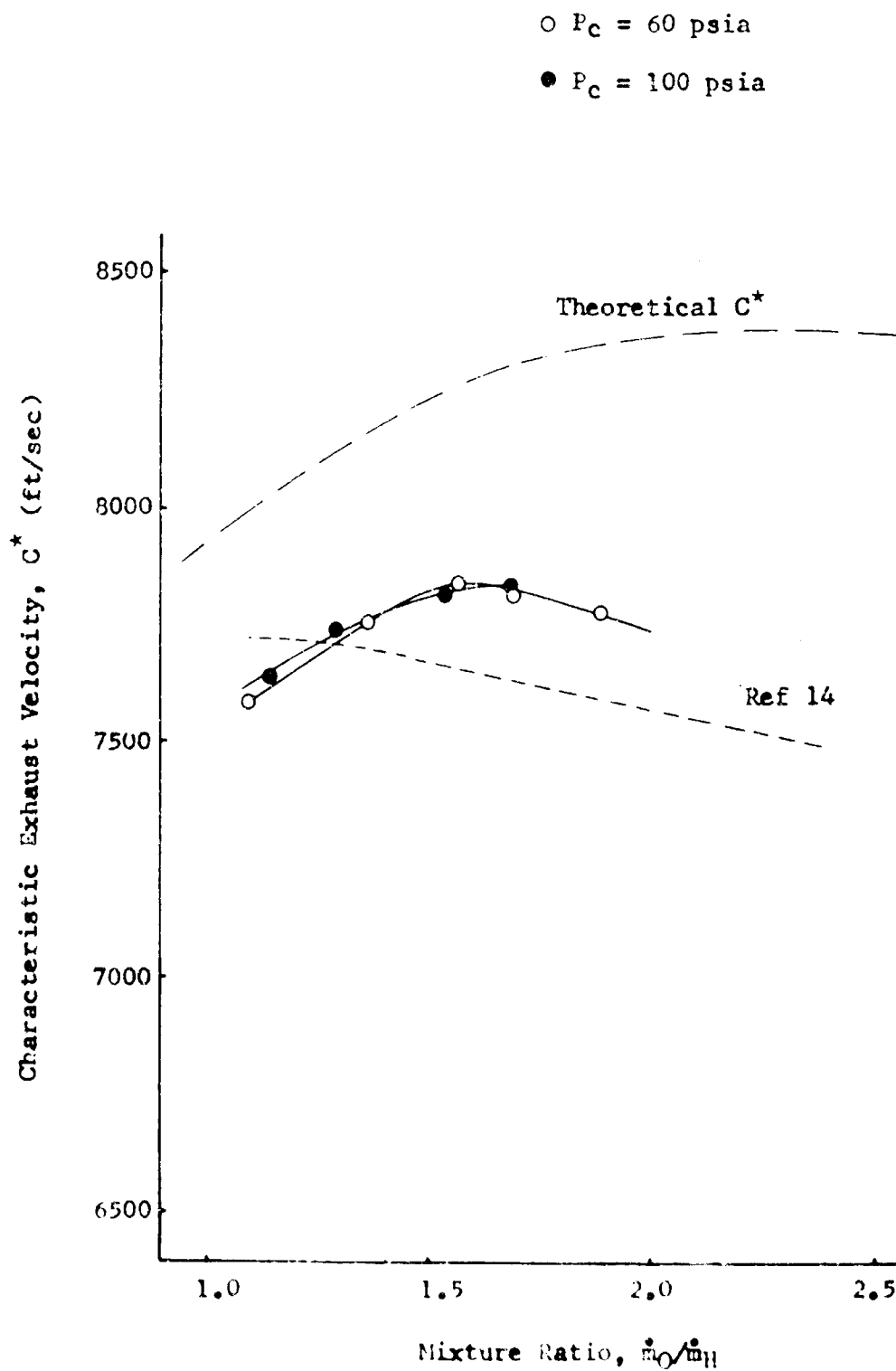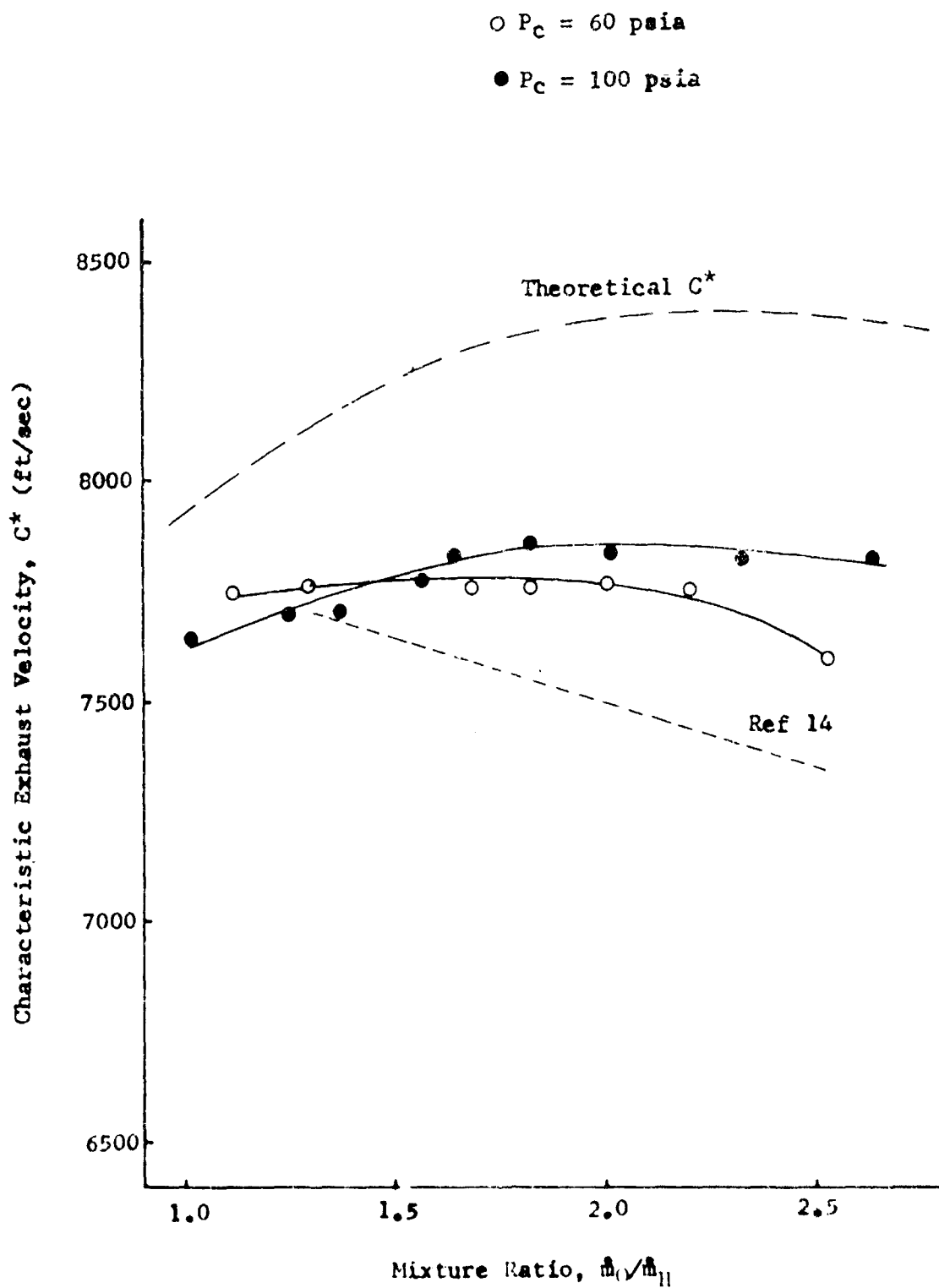
Figure 15

The Effect of Chamber Pressure on C^*
for the L^*76 (Two Inch Extension) Engine

Figure 16

The Effect of Chamber Pressure on C^*
for the L*92 (Three Inch Extension) Engine
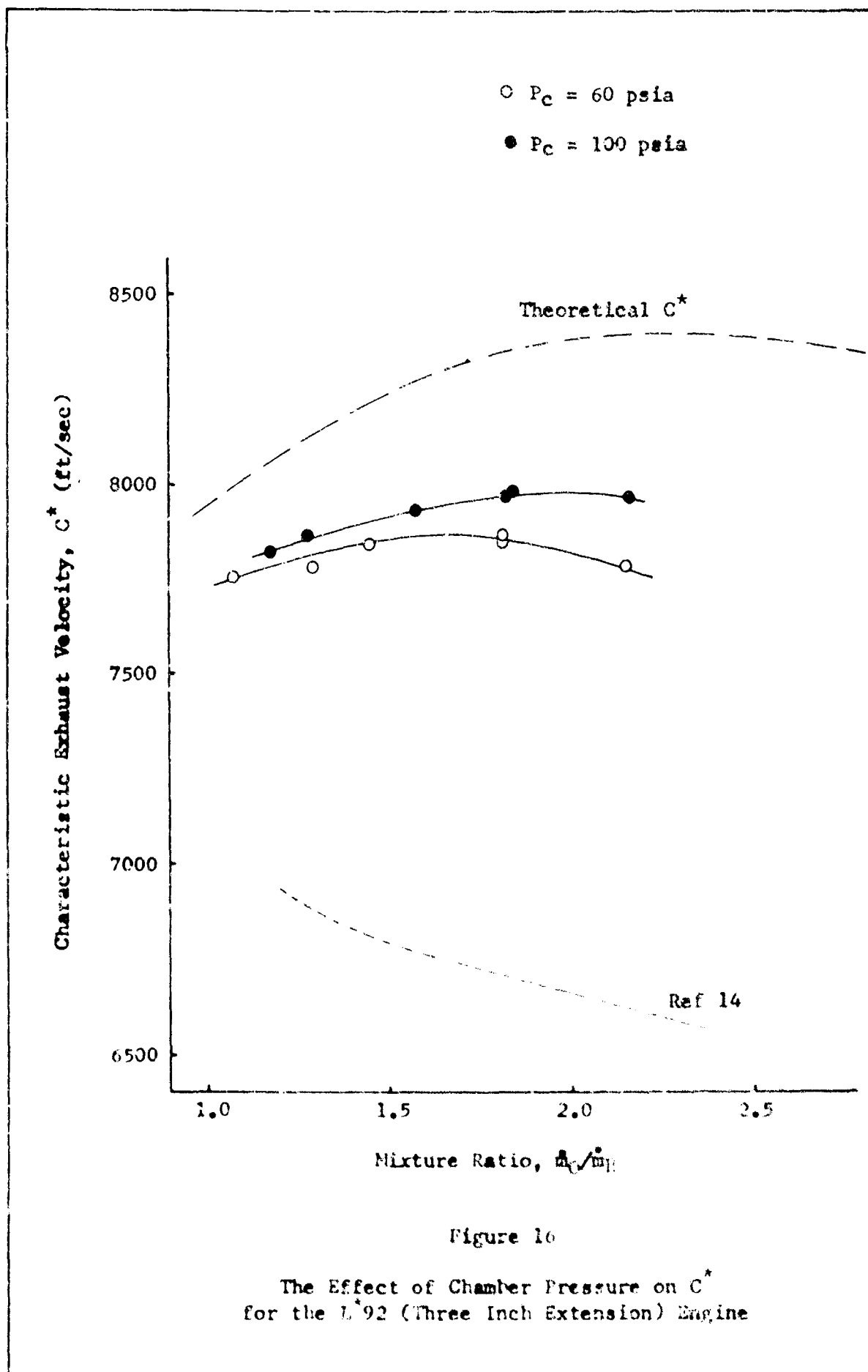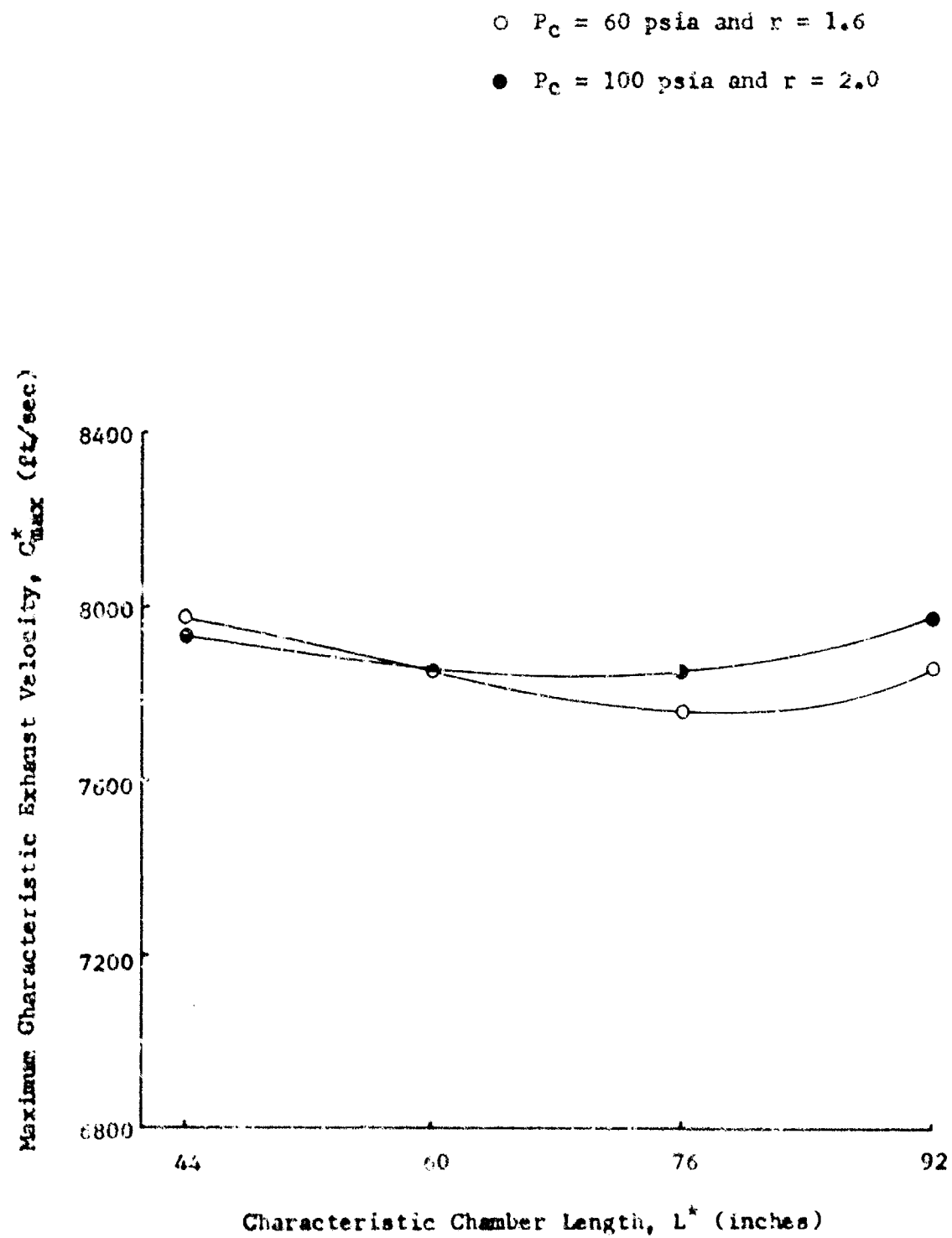
Figure 17

Maximum Characteristic Exhaust Velocity
vs Engine Configuration

Figure 18. Burning Velocities of Hydrogen-Oxygen
Flames at Various Chamber Pressures
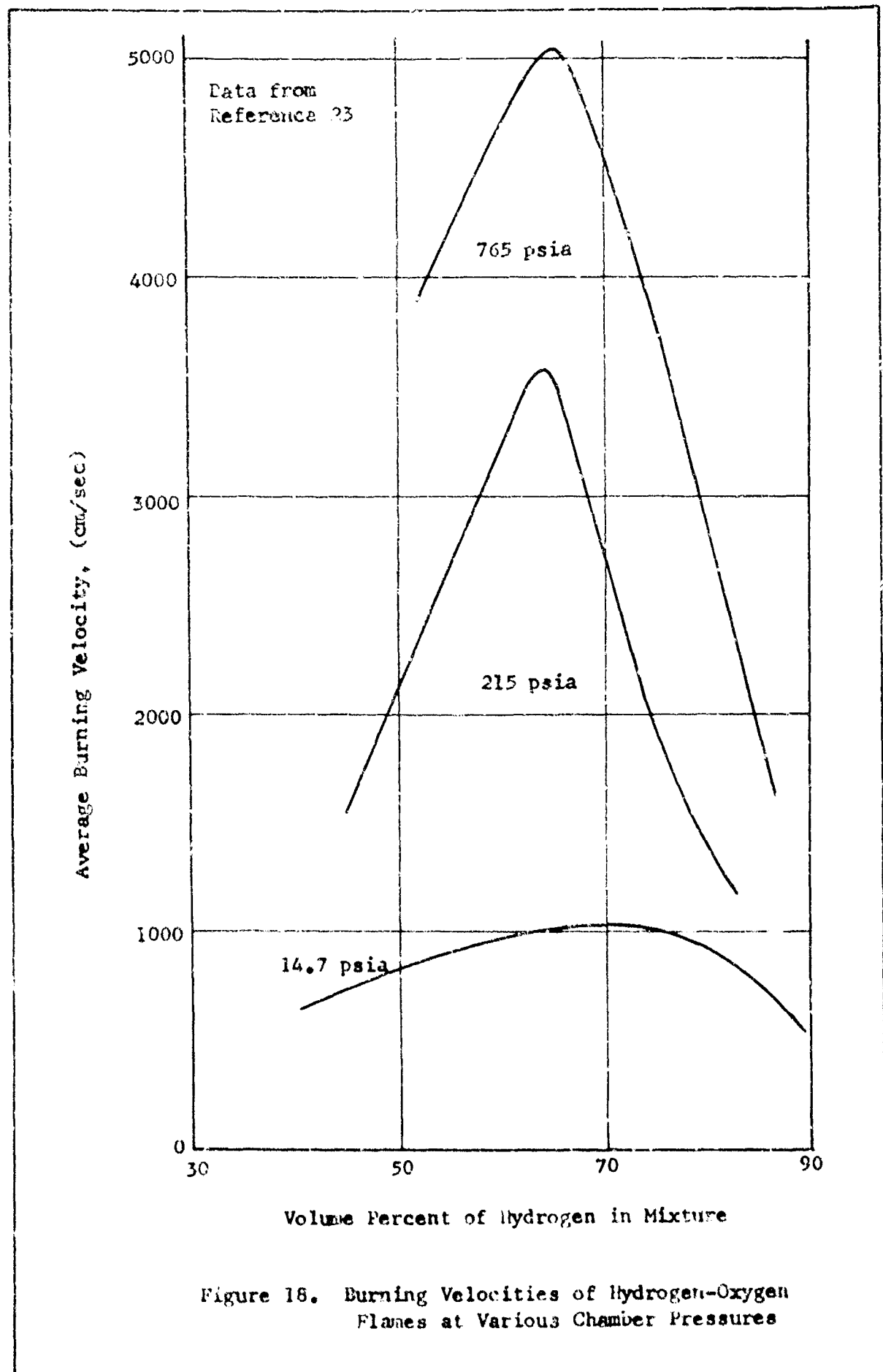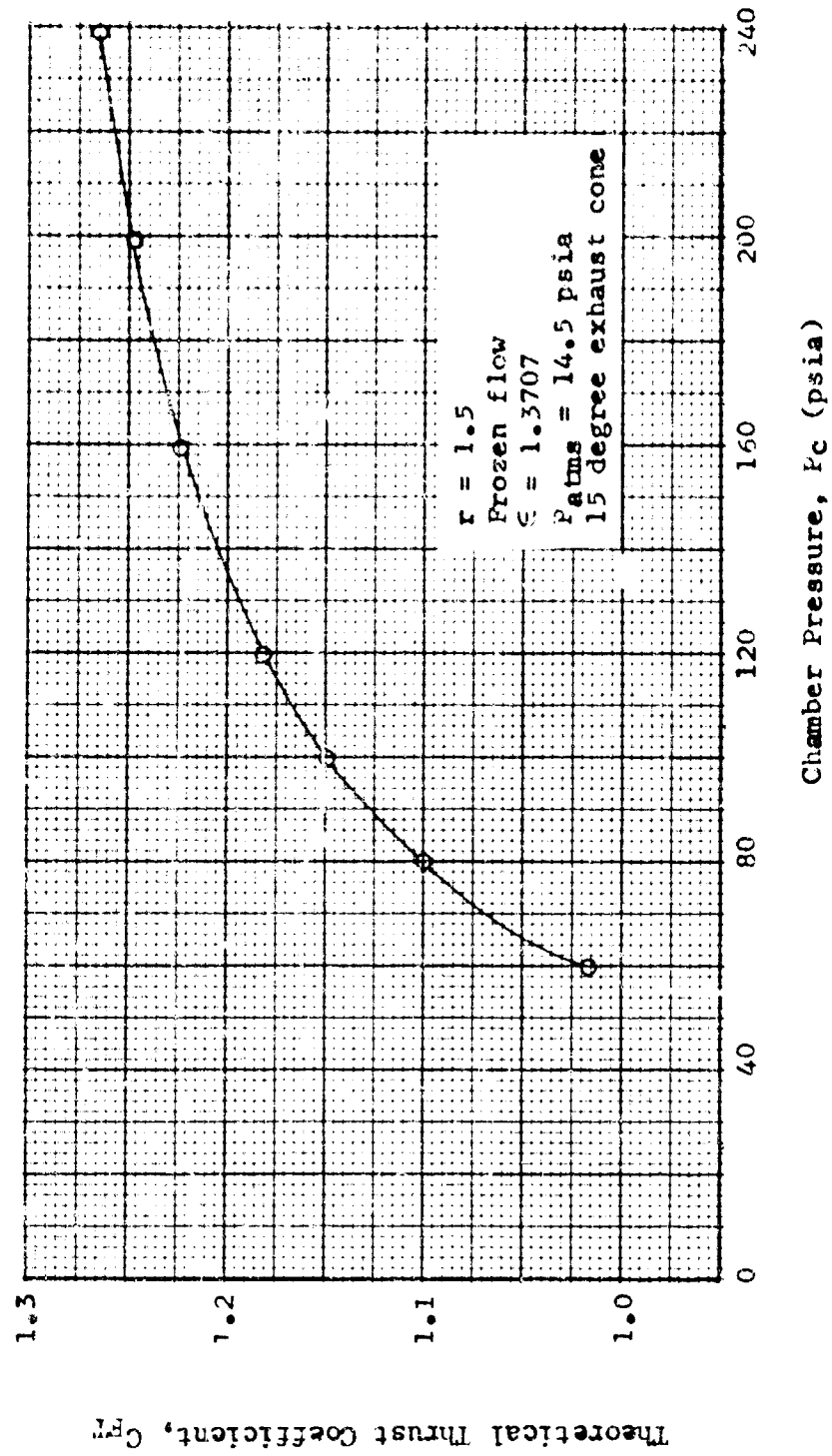
Figure 19

Theoretical Thrust Coefficient

Figure 20

Experimental Thrust Coefficient
Quality Factors for Each Engine

Figure 21

Variation of Inside Wall Temperature with Time

Figure 22

Hydrogen Feedline Pressure vs
Feedline Differential Pressure

Figure 23

Oxygen Feedline Pressure vs
Feedline Differential Pressure

List of Tables

TABLE I

TEST DATA SUMMARY FOR L*44 ENGINE (RUNS 44 TO 68)

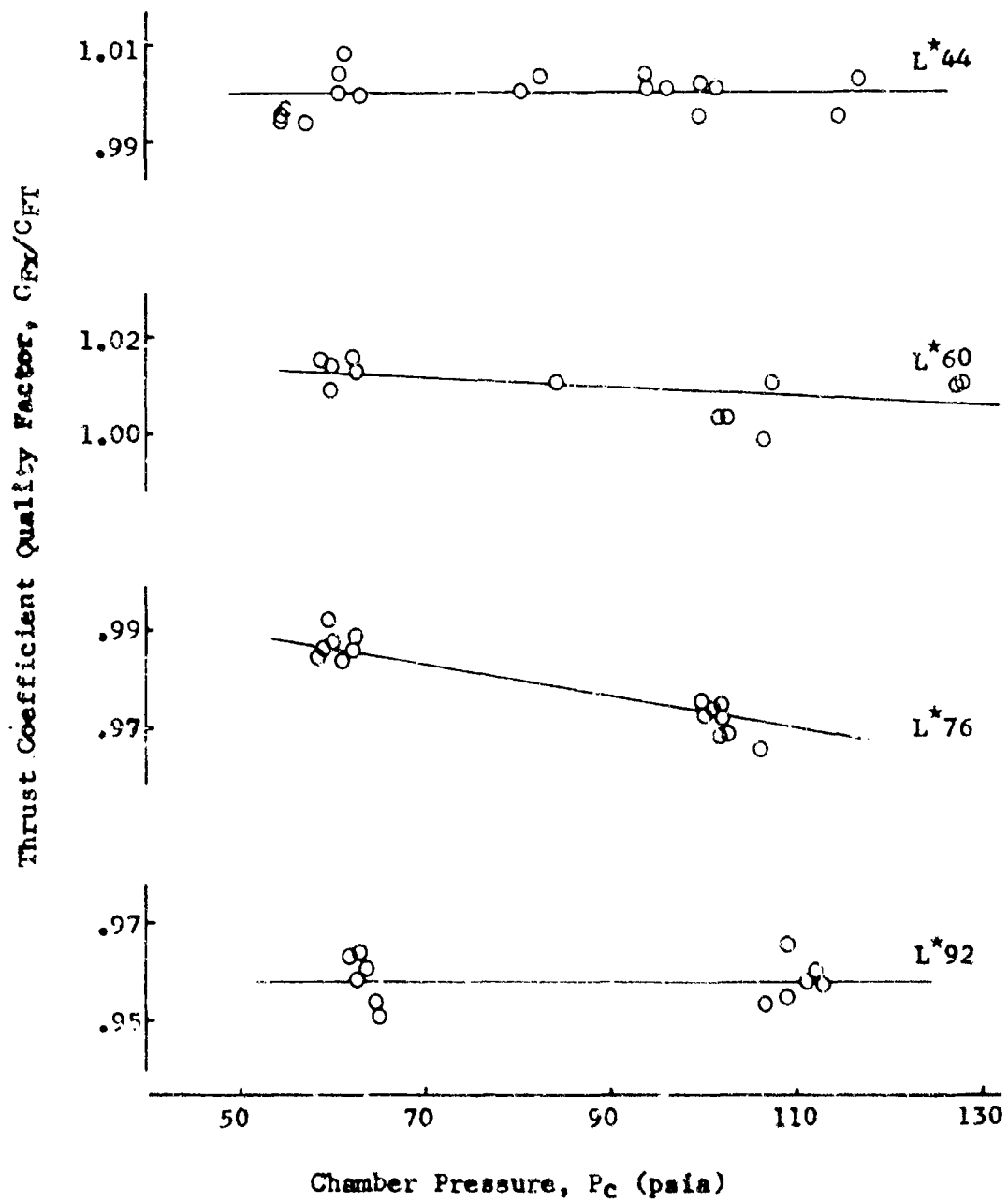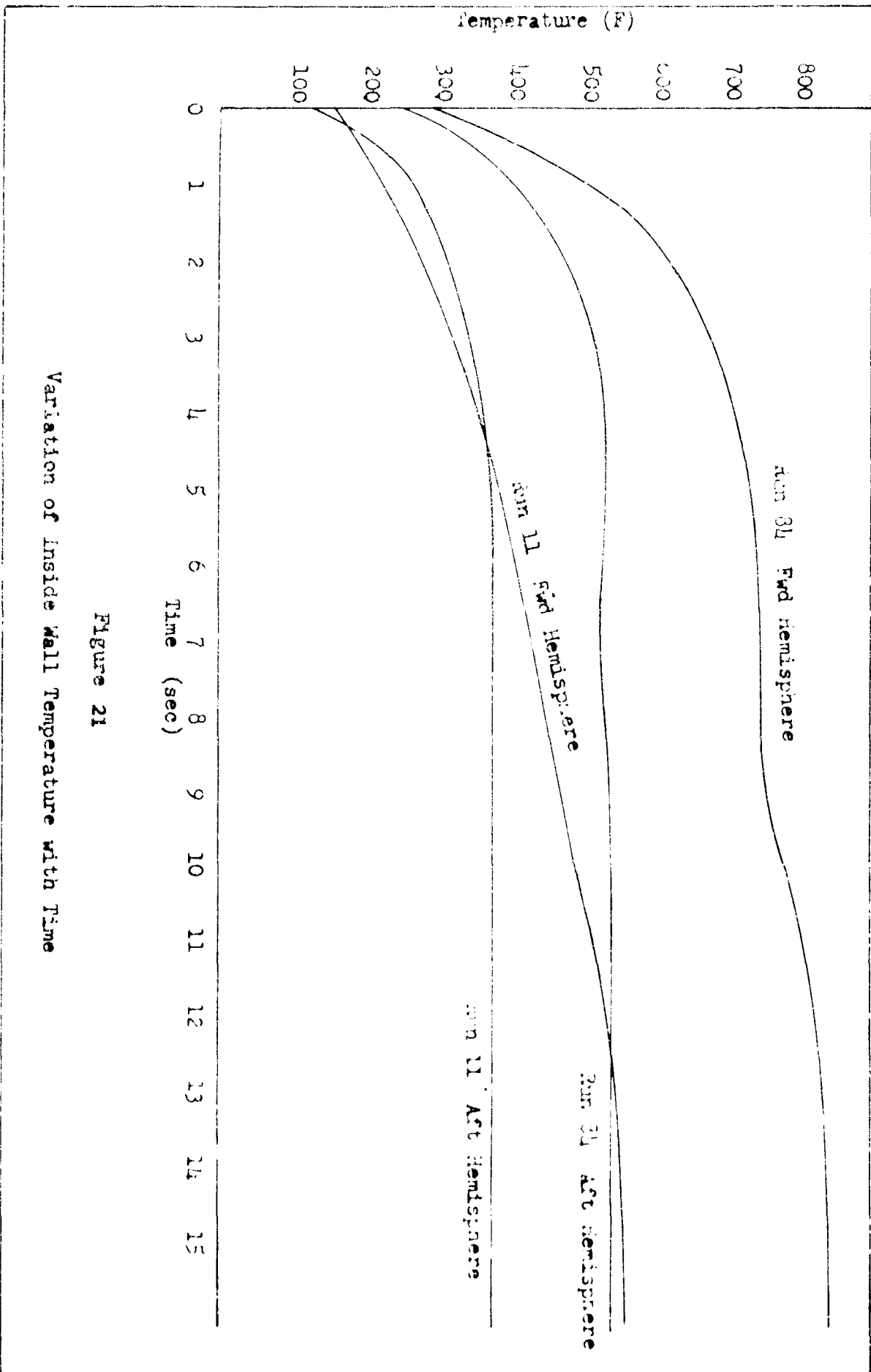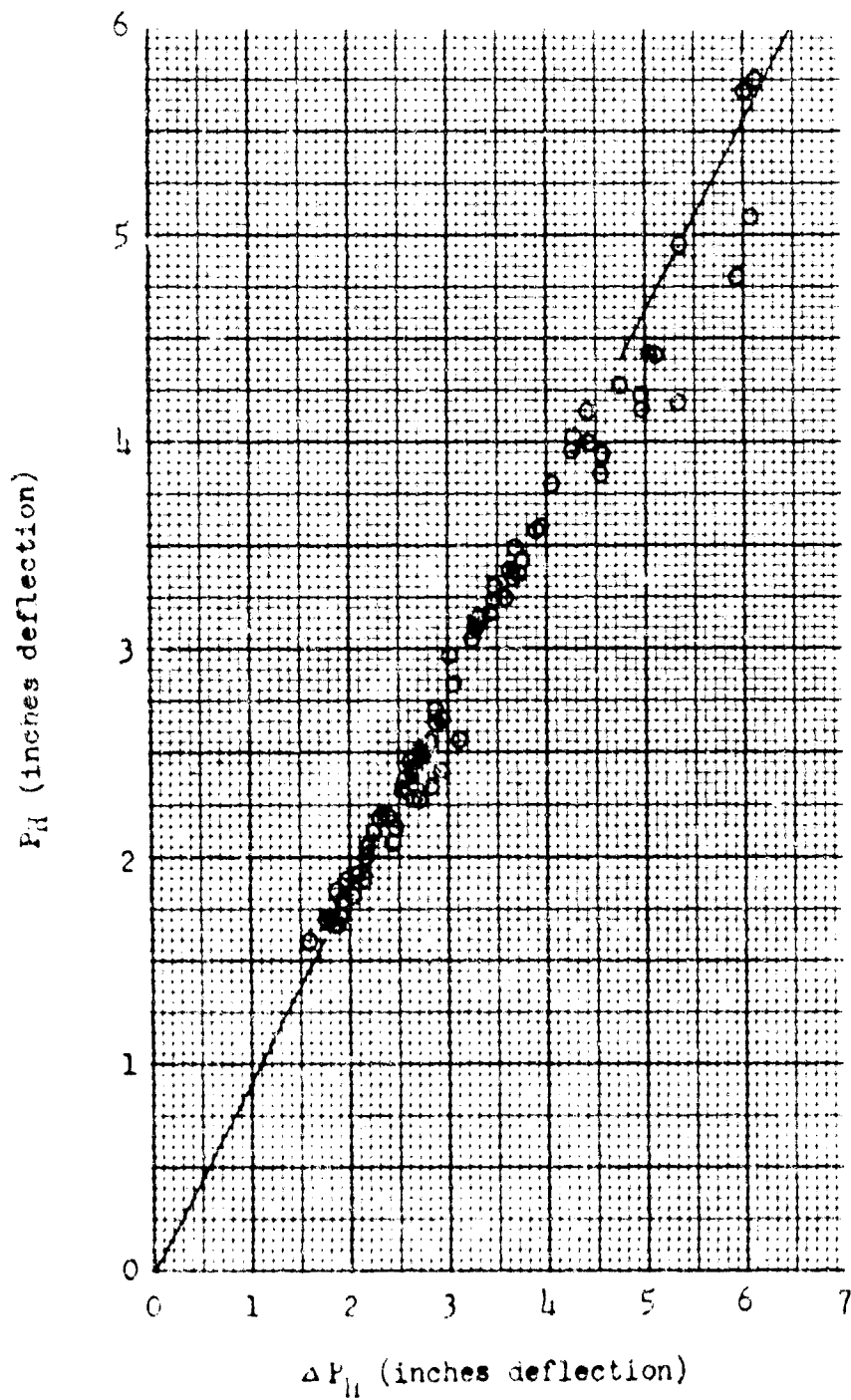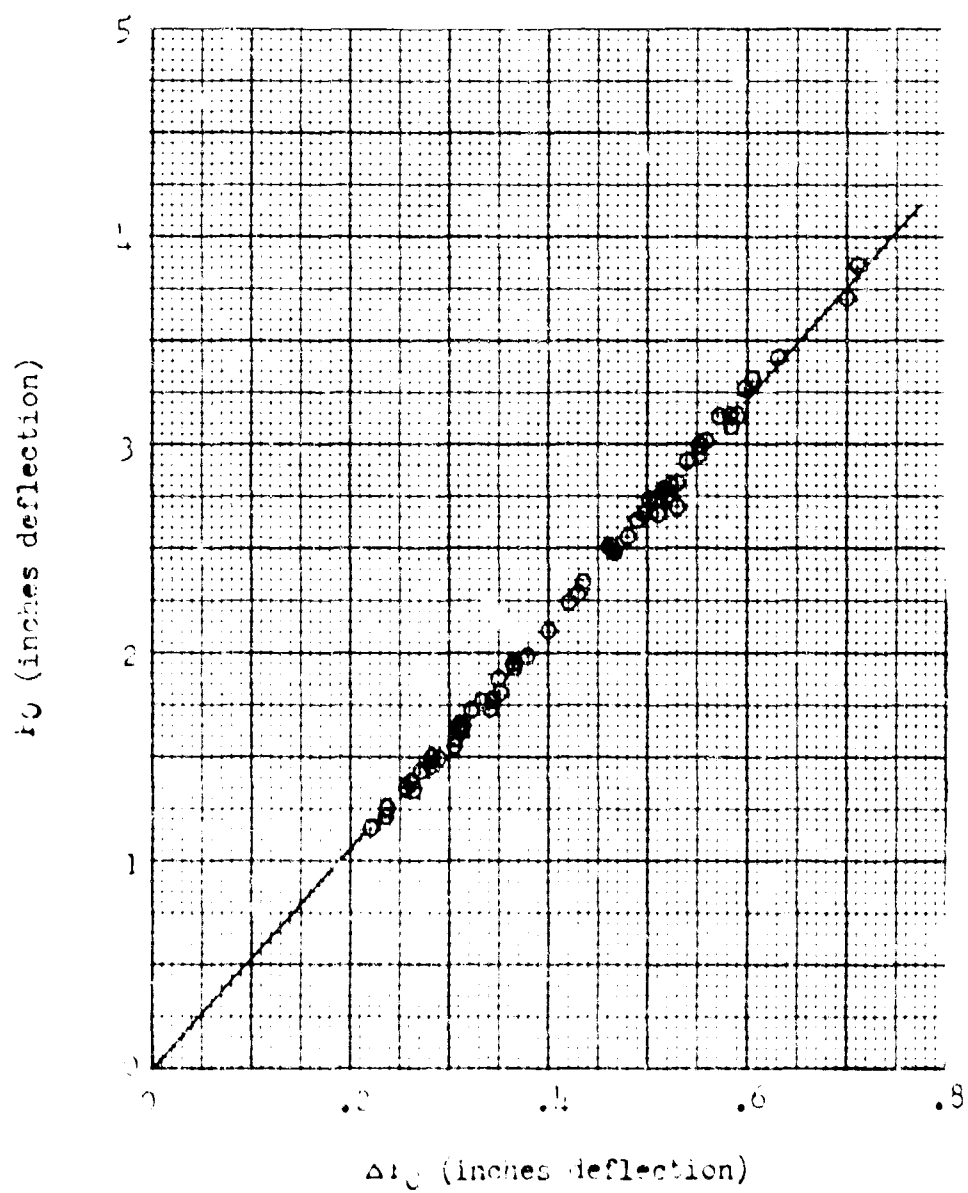| RUN NR.	PC	MIX RATIO	THR	H2 FLOW	O2 FLOW	C*	CF	ISP	O/O C*	O/O CF	O/O ISP
57	57.1	.94	45.3	.0980	.0925	7683.8	.996	237.9	97.4	99.4	96.9
68	54.2	.96	42.2	.0924	.0887	7630.6	.977	232.9	97.1	99.4	96.5
67	54.2	1.14	42.2	.0834	.0955	7768.2	.977	235.9	96.9	99.5	96.4
45	61.3	1.23	50.4	.0900	.1112	7814.9	1.032	250.8	96.8	100.8	97.6
56	63.1	1.25	51.9	.0916	.1145	7846.3	1.032	251.8	97.0	99.9	97.0
66	54.9	1.35	43.0	.0758	.1029	7877.1	.983	240.7	96.6	99.6	96.2
53	60.4	1.70	49.0	.0720	.1226	7958.9	1.018	251.8	95.6	100.0	95.6
52	60.6	1.91	49.4	.0679	.1300	7853.2	1.023	249.8	93.9	100.4	94.4
46	80.1	1.19	70.2	.1202	.1433	7991.8	1.100	266.5	96.8	100.0	95.9
65	82.2	1.61	72.5	.1030	.1667	7807.8	1.108	268.9	94.1	100.3	94.5
47	95.9	1.13	87.2	.1468	.1683	7749.7	1.142	275.2	96.8	100.1	96.9
61	114.4	1.19	106.6	.1722	.2050	7769.8	1.170	282.7	96.6	99.5	96.1
62	116.7	1.24	109.9	.1721	.2144	7737.9	1.183	284.5	95.8	100.3	96.1
50	99.4	1.24	91.1	.1450	.1810	7814.8	1.150	279.4	96.6	100.7	96.8
64	93.5	1.26	84.9	.1363	.1729	7749.2	1.139	274.5	95.7	100.4	95.1
63	93.8	1.50	85.0	.1220	.1838	7864.5	1.136	277.8	95.4	100.1	95.5
49	99.2	1.71	90.2	.1186	.2032	7903.1	1.140	280.2	94.9	99.5	94.5
48	101.2	2.21	92.8	.1021	.2265	7891.5	1.151	282.5	94.1	100.1	94.2

TABLE II

TEST DATA SUMMARY FOR L*60 ENGINE (RUNS 69 TO 84)

RUN NR.	PC	MIX RATIO	THR	H2 FLOW	O2 FLOW	C*	CF	ISP	O/O C*	O/O CF	O/O ISP
76	58.6	1.10	47.8	.0939	.1037	7596.1	1.024	241.8	95.1	101.5	96.5
77	59.8	1.36	48.8	.0833	.1140	7772.1	1.025	247.6	95.2	100.9	96.1
78	61.9	1.56	51.4	.0788	.1235	7848.2	1.042	254.2	94.9	101.6	96.5
79	59.8	1.68	49.1	.0729	.1231	7820.1	1.030	250.3	94.0	101.4	95.4
80	62.1	1.88	51.4	.0708	.1336	7786.9	1.039	251.5	93.2	101.3	94.4
69	84.2	1.31	74.5	.1197	.1576	7783.9	1.111	268.8	95.8	100.0	95.8
84	107.2	1.14	99.5	.1679	.1915	7647.5	1.265	277.0	95.4	100.1	95.5
73	106.2	1.29	98.1	.1529	.1985	7744.2	1.159	279.1	95.4	99.9	95.3
74	102.6	1.53	94.6	.1330	.2037	7812.8	1.157	281.0	94.6	100.3	95.0
75	101.2	1.68	93.1	.1234	.2079	7830.5	1.154	280.9	94.2	100.3	94.5
83	127.6	1.07	122.6	.2036	.2193	7792.5	1.206	289.8	97.0	101.0	98.1
82	127.8	1.17	122.6	.1945	.2286	7738.7	1.204	289.6	96.3	101.0	97.3
72	147.2	1.24	143.2	.2170	.2712	7730.1	1.220	293.3	95.6	100.0	95.7
71	150.8	1.30	147.9	.2143	.2807	7806.5	1.231	298.8	96.1	100.9	97.0

TABLE III

TEST DATA SUMMARY FOR L*76 ENGINE (RUNS 85 TO 101)

RUN NR.	PC	MIX RATIO	THR	H2 FLOW	O2 FLOW	C*	CF	ISP	O/C C*	O/O CF	O/O ISP
93	60.3	1.11	48.2	.0942	.1054	7749.3	1.002	241.4	96.9	98.3	95.3
94	58.6	1.29	46.4	.0843	.1090	7763.7	.995	240.1	95.7	98.6	94.4
95	59.6	1.68	47.5	.0735	.1236	7751.5	1.000	241.1	93.2	98.7	92.1
96	58.2	1.82	45.8	.0681	.1243	7753.7	.988	238.3	92.9	98.4	91.4
97	58.9	2.00	47.0	.0647	.1295	7777.1	1.001	241.9	92.9	99.2	92.2
98	61.7	2.19	49.6	.0638	.1403	7754.2	1.009	243.1	92.5	98.6	91.2
99	62.1	2.52	50.2	.0594	.1502	7596.9	1.014	239.5	90.6	98.9	89.7
87	101.7	1.02	90.7	.1686	.1727	7639.3	1.119	265.9	96.2	97.1	93.5
88	101.4	1.24	94.6	.1506	.1870	7697.1	1.115	266.9	95.3	96.8	92.3
100	106.0	1.37	94.6	.1486	.2040	7698.9	1.120	268.1	94.3	96.5	91.0
89	101.6	1.56	90.7	.1303	.2045	7775.6	1.121	271.1	94.0	97.4	91.6
90	99.3	1.64	88.5	.1227	.2019	7837.7	1.119	272.7	94.4	97.5	92.1
86	109.7	1.82	100.4	.1268	.2309	7858.7	1.149	280.7	94.2	98.5	92.8
91	107.7	2.01	89.8	.1092	.2203	7829.5	1.119	272.4	93.5	97.4	91.1
92	104.0	2.32	88.8	.0986	.2290	7820.1	1.115	271.1	93.2	97.2	90.7
101	103.1	2.63	90.7	.0919	.2421	7832.8	1.115	271.4	93.6	96.8	90.6

TABLE IV

TEST DATA SUMMARY FOR L*92 ENGINE (RUNS 102 TO 113)

RUN NR.	PC	MIX RATIO	THR	H2 FLOW	O2 FLOW	C*	CF	ISP	O/O C*	O/C CF	O/O ISP
108	64.3	1.08	50.7	.1019	.1106	7749.1	.991	238.8	97.1	95.3	92.6
109	63.2	1.30	49.9	.0903	.1182	7768.0	.992	239.5	95.7	96.0	91.9
110	61.6	1.45	48.3	.0821	.1196	7830.3	.985	239.7	95.3	96.2	91.7
111	64.4	1.82	50.6	.0744	.1357	7856.6	.986	240.8	94.1	95.0	89.4
112	62.1	1.82	48.6	.0720	.1314	7831.0	.981	238.9	93.8	95.6	89.7
113	62.5	2.16	49.3	.0651	.1408	7776.2	.990	239.4	92.7	96.3	89.4
102	108.9	1.18	97.7	.1637	.1935	7810.6	1.126	273.4	97.1	96.5	93.8
103	106.4	1.28	93.9	.1519	.1950	7859.6	1.108	270.6	97.0	95.3	92.5
104	108.7	1.58	96.3	.1360	.2156	7922.6	1.112	273.9	95.7	95.4	91.4
105	110.6	1.83	98.5	.1257	.2306	7957.1	1.118	276.6	95.3	95.7	91.3
106	112.8	1.84	100.7	.1275	.2353	7965.0	1.121	277.6	95.4	95.7	91.4
107	114.7	2.16	99.7	.1137	.2462	7954.0	1.121	277.2	94.9	96.0	91.1